TECHNO-ECONOMIC ANALYSIS OF FULL-SCALE PRESSURE RETARDED OSMOSIS PLANTS

A Thesis

by

ELIZABETH IJEOMA OBODE

Submitted to the Graduate and Professional School of
Texas A&M University
in partial fulfillment of the requirements for the degree of

MASTER OF SCIENCE IN CHEMICAL ENGINEERING

Chair of Committee,	Ahmed Abdel-Wahab
Co-Chair of Committee,	Marcelo Castier
Committee Members,	Eyad Masad
Head of Department,	Patrick Linke

December 2021

Major Subject: Chemical Engineering

ABSTRACT

Pressure retarded osmosis (PRO) is a power generation process that harnesses the salinity gradient between two bodies of water. In literature, the most dominant example of this type of energy is from the mixing of sea water and river water. However, as the first pilot plant of this type proved, this pair is not sufficient to generate enough energy to offset the cost of generation and is unfeasible economically.

This work aims to assess the techno-economic feasibility of both single stage and multistage PRO design configurations using hypersaline solution (as Draw) and Seawater (as feed). The hypersaline draw of focus is produced water which is obtained from oil and gas reservoirs. For this work, a PRO simulator is used, which was developed at Texas A&M University at Qatar. It uses the Q-electrolattice Equation of State (EoS) and a mass transfer model to determine equipment parameters, pump and turbine powers as well as stream properties of interest. This work extends the capabilities of the simulator to handle economic calculations as well as the decision-making criteria that points to profitability or lack thereof. Its capabilities were also extended to interface with DAKOTA – a tool to aid in sensitivity analysis and mathematical optimization.

Using Levelized Cost of Electricity (LCOE) as the techno-economic parameter of interest, this work shows that energetic and economic optimum occur at different system conditions, quantifies the effect of membrane nonidealities on LCOE, shows the optimal plant dimensions and system conditions to operate a PRO plant using both ideal and real membranes and compares PRO to other renewable energy technologies. It also shows results of the energetic and economic performance of multistage systems.

DEDICATION

To all researchers working to avoid catastrophe due to climate change. May we win.

ACKNOWLEDGEMENT

I would like to thank Dr. Ahmed Abdel-Wahab for giving me the opportunity to work on this project and for his guidance throughout. I would like to appreciate Dr. Marcelo Castier for always being available with insights and feedback during the course of this project. This work would not have been possible without them. I would like to thank Dr. Eyad Masad for his inputs during the course of this work.

I would like to thank Dr. Lateef Akinkpelu and Juwon Ifalade for their conversations and insights on economic decision making under uncertainty. I would like to thank Husnain Manzoor and Saly Matta for their guidance on the set-up of the simulator.

I am thankful to my Mom and Dad for always cheering me on.

CONTRIBUTORS AND FUNDING SOURCES

Contributors

This work was supervised by a thesis committee consisting of Professor Ahmed Abdel-Wahab and Professor Marcelo Castier of the Chemical Engineering Program, and Professor Eyad Masad of the Mechanical Engineering Program. The routines for the Equation of State used to develop the process simulator was provided by Dr. André Zuber. The parameter fitting routines were provided by Dr. Marcelo Castier and the routine for the calculation of Osmotic Pressure was developed by Dr. Muaz Salem. Husnain Manzoor developed the flat sheet membrane routine and Saly Matta developed the spiral wound membrane routine. All other work conducted for the thesis was completed by the student.

Funding Sources

This work was made possible in part by a grant from the National Priorities Research Program (NPRP) of Qatar National Research Fund under Grant Number NPRP10-1231-160069 and in part by the financial support from ConocoPhillips Global Water Sustainability Center (GWSC).

NOMENCLATURE

A	water permeability of the membrane
ΔA^{MTC}	contribution to Helmholtz energy from Matted-Tavares-Castier (MTC) EoS
ΔA^{MSA}	contribution to Helmholtz energy from the mean spherical approximation
ΔA^{Born}	contribution to Helmholtz energy calculated from Born Equation
A_m	wrea of the membrane
A^R	residual Helmholtz free energy
B	Salt permeability of the membrane
CC	Capital cost of an equipment
C_{OPEX}	total operating cost
$C_{F,b}$	concentration of the bulk feed solution
$C_{D,b}$	concentration of the bulk draw solution
C_{CAPEX}	total Capital cost
CEPCI	Chemical Engineering Plant Cost Index
D	bulk diffusion coefficient
E	energy produced by the plant per year
h	molar enthalpy
i	discounting factor
J_s	reverse salt flux
J_W	Water flux across the membrane

k	Mass transfer co-efficient
LCOE	Levelized Cost of Electricity
$\dot{m}_{P,s}$	salt molar flowrate
$\dot{n}$	molar flowrate
n^F	feed molar flowrate
n^D	draw molar flowrate
n_w^D	molar flowrate of water in the draw stream
n_s^D	molar flowrate of salt in the draw stream
n_w^F	molar flowrate of water in the feed stream
n_s^F	molar flowrate of salt in the feed stream
N	total life of the plant
OC	Operating cost
S	structural parameter of the membrane support layer
s	molar entropy
$\dot{V}_{draw}$	volumetric flowrate of the draw
$\dot{V}_{feed}$	volumetric flowrate of the feed
$\dot{V}_P$	water permeate flowrate
$\dot{V}_{PX}$	volumetric flowrate through the pressure exchanger
V_m	molar volume of the solution
$\dot{W}_{shaft,rev}$	reversible shaft power

$\dot{W}_{shaft}$	Shaft Power
$\dot{W}_{system}$	net power produced – difference between pump and turbine powers
x	mole fraction

Greek letters

π	Osmotic Pressure of the solution
$\pi_{D,b}$	osmotic pressure of the bulk draw solution
$\pi_{F,b}$	osmotic pressure of the bulk feed solution
η	efficiency
ϕ	ratio of feed flowrate to total flowrate

Subscripts

w	water
s	salt

TABLE OF CONTENTS

LIST OF FIGURES

LIST OF TABLES

1 INTRODUCTION

Increasing energy demand and anthropogenic climate change have led to increased research in alternative sources of energy [1]. Among these technologies are solar and wind power, which has experienced increased adoption due to sufficient economic viability to attain grid parity [2][3]. Grid parity refers to the point where renewable energy technologies can produce power at the same cost or lower than that obtainable from conventional grids powered by hydrocarbons [4].

Salinity gradient energy, which refers to the energy of mixing solutions with different salt concentrations, has also enjoyed increased research interest [5]. Salinity gradient energies can be harnessed through technologies that include reverse electrodialysis (RED) [6], capacitive mixing [7], hydrogel swelling [8], and pressure retarded osmosis [9].

Pressure retarded osmosis (PRO), which is the focus of this work, makes use of a semi-permeable membrane between two solutions of different concentrations. Due to osmosis, water molecules move through the membrane from the solution of low concentration to that with the higher concentration. The process operates in such a way that the pressure on the side of the higher salt concentration (draw solution) is higher than the pressure on the side of the lower salt concentration (feed solution). The value of this hydraulic pressure difference is smaller than the osmotic pressure difference between the draw and feed solutions. In this way, there is an osmotic flow of solvent – water, typically – from the feed to the draw solution. These two effects – increase in pressure of draw solution and its flow rate enable the generation of mechanical power in a hydroturbine, which extracts power from the pressurized draw solution [5].

1.1 AIM OF THIS WORK

This work aimed to investigate the economic feasibility of PRO to produce energy using hypersaline draw solutions, and evaluate the performance of different PRO configurations. Also, the work includedcomparison of this technology with other renewable energy technologies, analyzing the sensitivity of costs to selected model parameters, and determining optimal operating conditions.

1.2 THESIS OVERVIEW

Chapter 2 reviews the existing body of work on PRO, dividing the literature broadly into three distinct timelines – early-stage development, an optimistic period that ends with the close of the first pilot plant, and a cautious period that looks at PRO process scalability. Also, an overview of the simulator and the process for membrane development already embedded in the simulator is provided. Additionally, this chapter discusses existing literature on cost estimation methods and types.

Chapter 3 presents the details of the methodology used in developing the techno-economic framework. Equations underlying the development of each equipment and associated costing models are included.

Chapter 4 presents results showoff this research on how the current state-of-the-art PRO process compares with other renewable energy technologies, the sensitivity of various process variables to LCOE (levelized cost of electricity), proposed optimal membrane properties, and comparison of PRO to other renewable energy technologies. Multistage analysis is carried out to asssess whether incremental power gained from additional equipment justifies the increased capital expenditure involved.

Chapter 5 gives the conclusions and recommendations for future work.

2 LITERATURE REVIEW

2.1 THE OSMOTIC PROCESS

In general, osmotic processes occur as a result of the difference in chemical potential of each component in two solutions separated by a semi-permeable membrane. Depending on the magnitude of osmotic pressure difference ($\Delta\pi$) and the magnitude of hydraulic pressure (ΔP), three types of osmotic processes can be identified as shown in Figure 1.

1. Forward Osmosis describes the 'natural tendency' of solvent in a solution of lower concentration to move to a solution of higher solute concentration, with $\Delta P=0$.
2. Reverse Osmosis in which an external hydraulic pressure is applied to the more concentrated solution to force out freshwater, leaving behind solute, with $\Delta P > \Delta\pi$.
3. Pressure Retarded Osmosis describes the process in which an external hydraulic pressure is applied to a highly concentrated solution (called draw solution) and the less concentrated solution (called feed solution) is allowed to permeate through the membrane towards the draw solution. However, permeate water flow is retarded by applying hydraulic pressure difference lower than osmotic pressure difference. The excess water is then channeled to a turbine to produce power. In this case, $0 < \Delta P < \Delta\pi$

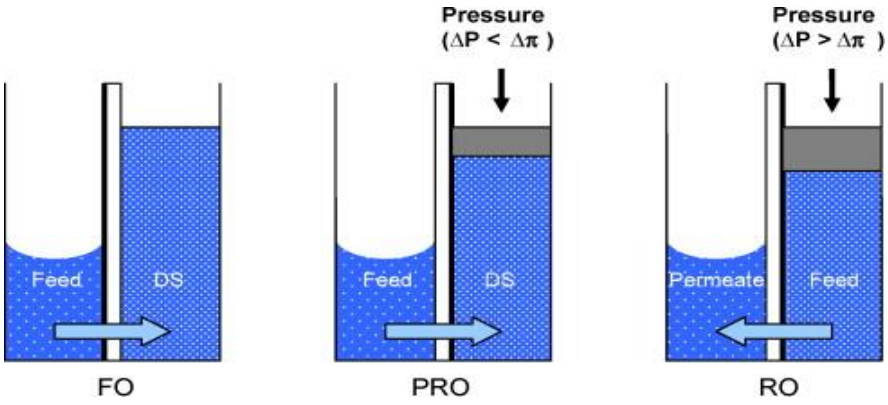

Figure 1:Schematic of Different Osmotic Processes. Reprinted with permission from Achilli et al. [10]. Copyright 2009 Elsevier

2.2 DEVELOPMENT OF PRO

The development of PRO can be divided into three broad timelines –

1. Early stages– a period which ranged from 1954 to 1990
2. Optimism period – a period which ended in 2014 with the closedown of the first PRO plant
3. Cautious times – a period which birthed a more critical look at the scalability of PRO processes

2.2.1 EARLY STAGES

Utilization of salinity gradient as an energy source was first reported by Pattle [11] who posits that the energy of mixing of the river and sea is equivalent to the energy obtainable from a 680ft waterfall. In this same work, he proposes that the economics of this process hinges on how frequently the membranes need to be replaced.

In a series of two papers, Loeb [12] and Loeb et al. [13] reported the first techno-economic evaluation of the PRO process. This was also the first mention of hypersaline pairing as they envisioned the Dead Sea and Jordan River as the draw and feed, respectively. This work also gave some insight into membrane qualities desired for hypersaline pairing as they reported membrane damage on contact with Dead Sea water. It also concluded that energy generation costs amount to $0.072/kWh under highly optimistic assumptions for the equipment costs and efficiency as well as increased capability of the membrane to resist fouling. In 2001, however, the author revised this estimation when he carried out an economic evaluation of the PRO process and concluded that the cost of energy generation is $0.09/kWh [14]. For this analysis, the capital cost was based on the capital cost for a Brackish Water Reverse Osmosis (BWRO) Plant of $320/($m^3$/day) which is the value gotten after a scale-down factor applied to correct for the location of the PRO plant. This is much less than the average cost per volume for a Sea

Water Reverse Osmosis plant of \$1,000(m^3/day) [15]. BWRO cost is not an adequate estimation of capital costs for PRO due to the absence of high pressure booster pumps [3].

Lee et al. [16] also carried out techno-economic evaluations but they assumed that all equipment and membrane costs are \$100/m^2. Thus, the model lacks the robustness needed to truly evaluate the PRO process. However, in this work, they also conclude that the seawater/wastewater pairing was economically unfeasible.

For an ideal membrane, the water flux (J_W) associated with transport across it can be given by equation 1 [16]. An ideal membrane is one with no concentration polarization or reverse salt flux.

$$J_W = A(\Delta\pi - \Delta P) \tag{1}$$

where A represents water permeability.

The relationship for water flux in a non-ideal membrane by incorporating salt leakage and internal concentration polarization was developed by Lee et al. [16]

$$J_W = A\left(\pi_{D,b}\frac{1-\frac{C_{F,b}}{C_{D,b}}exp(J_wK)}{1+\frac{B}{J_w}[exp(J_wK)-1]} - \Delta P\right) \tag{2}$$

where $\pi_{D,b}$ represents the osmotic pressure of the bulk draw solution, $C_{F,b}$ and $C_{D,b}$ represent the concentration of the bulk feed and draw solutions respectively. B represents salt permeability and K is the mass transfer coefficient.

In this same work, they also presented a preliminary economic analysis where they concluded that capital costs of the PRO plant depend on three main factors: the salinity gradient pairing used, the membrane characteristics that determine the maximum allowable pressure, and the power output per unit area as well as installed membrane costs. They also concluded that the

economic viability of seawater/freshwater pairing would be possible only with a membrane that is impermeable to salt (such that B~0).

2.2.2 OPTIMISTIC PERIOD

Interest in PRO picked up steam after the Kyoto Meeting in 1997 and with the famous question by Sidney Loeb 'Energy production at the Dead Sea by pressure-retarded osmosis: challenge or chimera?'[17] where he concluded optimistically that the cost of electricity generated would be in the range of $0.017/kWh – $0.058/kWh, with the added benefit of refilling the Dead Sea with discharge brine. In 2009, Achilli et al. [10] developed a model which incorporated dilutive external concentration polarization (ECP) into the water flux model.

$$J_W = A\left(\pi_{D,b}\, exp\left(-\frac{J_w}{k}\right)\frac{1-\frac{\pi_{F,b}}{\pi_{D,b}}exp(J_wK)\, exp\left(\frac{J_w}{k}\right)}{1+\frac{B}{J_w}[exp(J_wK)-1]} - \Delta P\right) \tag{3}$$

where k is the mass transfer coefficient of the membrane and K represents the effect of ICP on water flux.

An alternative model was developed by Yip et al. [18], which simultaneously accounted for Internal Concentration Polarization (ICP) and dilutive External Concentration Polarization (ECP). This is the model most commonly used to simulate PRO processes and it is used in this work –

$$J_W = A\left(\frac{\pi_{D,b}\ exp\left(-\frac{J_w}{k_D}\right)-\pi_{F,b}\, exp\left(\frac{J_wS}{D}\right)}{1+\left(\frac{B}{J_w}\right)\left[exp\left(\frac{J_wS}{D}\right)-exp\left(-\frac{J_w}{k_D}\right)\right]} - \Delta P\right) \tag{4}$$

where $\pi_{D,b}$ and $\pi_{F,b}$ represents the osmotic pressure of the bulk draw and bulk feed solutions respectively, S represents the structural parameter of the membrane support layer and k_D is the boundary layer mass transfer co-efficient.

In 2008, researchers from Statkraft [19] published a report of the research progress made by the company in osmotic power and membrane technology and its outlook that investment in the technology would allow for a profitable margin. Gerstandt et al. [20] carried out more laboratory-scale research into developing a membrane that would give a power density of $5W/m^2$, also in preparation for the pilot plant deployment by Statkraft. In 2014, the pilot plant closed down due to insufficient power production, which was reportedly caused by reverse salt flux, membrane fouling, and concentration polarization [21]. The plant had achieved a total power output of 2kW with a membrane size of $2000m^2$ (power density of $1W/m^2$). The closedown of the pilot plant birthed a new phase in PRO research with more emphasis on the scalability of coupon scale parameters.

2.2.3 CAUTIOUS PERIOD – CRITICAL LOOK AT SCALABILITY

Feinberg et al. [22] assessed the scalability of both Reverse Electro Dialysis (RED) and PRO. They accounted for plant scale system losses which are not observable in lab-scale modeling and concluded that actual power density for PRO processes in full scale is much lower than those reported in literature via the extrapolation of laboratory-scale results. Interestingly, they concluded that maximum power density is not an adequate parameter to assess plant scale system feasibility.

A method of assessing the feasibility of different standalone PRO projects was proposed by Chung et al. [3]. They proposed a 'lower bound cost' scenario that leads to a decision on which scenarios are uneconomical. They concluded that only hypersaline water/river water or produced water/river water pairing with more than 18% wt draw solution salinity can compete with wind energy at its levelized cost of $0.074/kWh.

In keeping with the hypersaline water for draw solution, Khasawneh et al. [23] evaluated the feasibility of three proposed PRO projects on the Dead Sea – Red Sea water conveyance project

(RSDS). Their results showed that while all three projects were technically viable, only the third, with the Dead Sea/reverse osmosis brine, was economically feasible. Some location-specific economic evaluation of PRO processes has been reported in literature. Ansari et al. [24] evaluated the economic feasibility of deploying a PRO plant in Iran and concluded that the deployment of PRO is unfeasible in that location.

2.3 SIMULATOR OVERVIEW

The developed FORTRAN-based simulator has different subroutines/modules which correspond to the different equipment that makes up a PRO process. This modularity enables ease of implementing user-specific design configurations. The properties of each stream entering the process from the environment is user-specified and stream property calculations within the process are calculated using the Q-electrolattice Equation of State (EoS) developed by Zuber et al. [25]. The use of this advanced EoS enables accurate computation of stream thermodynamic properties and this gives more accurate osmotic pressure difference which is the driving force for energy production. The inputs required by the simulator as well as the corresponding units are shown in Table 1.

Table 1: Inputs needed by the simulator

INPUT	UNIT
Membrane	
Water Permeability (A)	$L/(m^2.h.bar)$
Salt Permeability (B)	$L/(m^2.h)$
Structural Parameter (S)	m
Slope of Structural Parameter against Pressure (used for pressure-dependent structural parameter)	m/Pa
Slope of Salt Permeability against Pressure (used for pressure-dependent salt permeability)	$L/(m^2.h.Pa)$
Mass Transfer Coefficient (k)	$L/(m^2.h)$
Area	m^2

Table 1: Inputs needed by the simulator (continued)

INPUT	UNIT
Equipment	
Draw Solution Pressure (supplied by draw pump)	Pa
Feed Solution Pressure (supplied by feed pump)	Pa
Pump Efficiency	%
Turbine efficiency	%
Pressure Exchanger (Depressurization efficiency)	%
Pressure Exchanger (Pressurization efficiency)	%
Stream Properties	
Draw and Feed Solutions Salinity	g/L
Draw and Feed Solutions Flowrate	m^3/s
Stream Temperature	K
Economics	
CEPCI Inflation Index for current year	-
Membrane cost	$\$/m^2$
Total Life of Membrane	Years
Total Plant Life	Years
Interest rate (i)	-
Electricity Selling Price	\$/kWh

2.3.1 EQUATION OF STATE

The van't Hoff equation which is the most widely used Equation of State in PRO literature [26], [27],[28] assumes ideal solution behavior which makes it unsuitable to model hypersaline solutions. When compared with experimental data, it was observed that at low salinities, it overpredicts the specific energy produced while it under-predicts the specific energy at high salinities [29].

In contrast, the developed simulator uses the Q-electrolattice EoS which is based on Helmholtz free energy expansion. The thermodynamic properties of interest which enable osmotic

pressure calculations are density, molar enthalpy, and molar entropy of the process stream as well as the chemical potential.

The residual Helmholtz free energy in the Q-electrolattice EoS is given by

$$A^R(T,V,n) = \Delta A^{MTC} + \Delta A^{Born} + \Delta A^{MSA} \quad (5)$$

Where ΔA^{MTC} represents the contribution of short-range non-electrostatic interactions to the Helmholtz free energy based on the Matted-Tavares-Castier (MTC) EoS [30].

$\Delta A^{Born}$is the contribution due to interaction between ion and solvent (ion-solvation effect) based on the Born Model [31].

ΔA^{MSA} is the contribution to Helmholtz energy due to long-range ion-ion interaction and is based on the mean spherical approximation [32].

To carry out the calculation of the real entropy and enthalpy of the system, residual properties gotten from the Q-electrolattice EoS are added to the ideal gas properties of the solution at the same temperature and pressure.

An electrolyte solution and a pure solvent at the same temperature separated by a semi-permeable membrane would reach equilibrium when the pressure difference is such that there is no flow of solvent from the pure solvent side to the solution side. In this way, at equilibrium, the fugacity of pure solvent and the solvent in the solution can be expressed as;

$$f_s^I = f_s^{II} \quad (6)$$

where f_s^I is the fugacity of the solvent in the solution and f_s^{II} is the fugacity of the pure solvent at the same temperature.

In terms of variables, equation) can be written as;

$$x_s^I \varphi^I_{s(T_s,P_s^I,x^I)} P_s^I = x_s^{II} \varphi^{II}_{s(T_s,P_s^{II},x^{II})} P_s^{II} \quad (7)$$

Where φ_s^I is the fugacity coefficient of the solvent in the solution and φ_s^{II} is fugacity coefficient for the pure solvent, x^I and x^{II} are the mole fractions in the solution and the pure solvent respectively.

By assuming that the pressure of the pure solvent is atmospheric, equation (7) is solved for P_s^I such that the equilibrium condition is satisfied. After equilibrium is reached, the osmotic pressure π of the solution can be calculated as;

$$\pi = P_s^I - P_s^{II} \quad (8)$$

The full development of this EoS and the mathematical expressions is given in the original work by Zuber et al. [25]

2.3.2 MEMBRANE IMPLEMENTATION

The simulator includes flat sheet membrane designed by Manzoor [33] and spiral wound membrane designed by Matta [34]. Full details of the work done can be found in their theses and in addition to that, the flat sheet membrane design can also be found in the paper published by Manzoor et al. [29].

However, this section presents a brief overview of the equations used in the design of the membrane, and Appendixes 1 and 2 presents the flowcharts for solving the membrane in co-current flow and countercurrent flow configuration respectively.

To calculate the water flux across, the mass transfer model developed by Yip et al. [18] is used.

$$J_w = A\left[\frac{\pi_{D,b}\, exp\left(-\frac{J_w}{k}\right) - \pi_{F,b}\, exp\left(\frac{J_w S}{D}\right)}{1 + \frac{B}{J_w}\left[exp\left(\frac{J_w S}{D}\right) - exp\left(\frac{J_w}{k}\right)\right]} - \Delta P\right] \quad (9)$$

where A (L/m^2.h.bar) is the water permeability, B is the salt permeability (L/(m^2.h)), k (L/(m^2.h)) is the membrane mass transfer coefficient, S(m) is the structural parameter of the membrane, D (m^2/s) is the bulk diffusion coefficient and $\pi_{D,b}$ and $\pi_{F,b}$ are osmotic pressures (bar) of the bulk draw and feed solutions respectively.

However, an imperfect membrane allows both water and salt to pass through it as shown in Figure 2. This gives rise to the reverse salt flux which can be computed by equation (10);

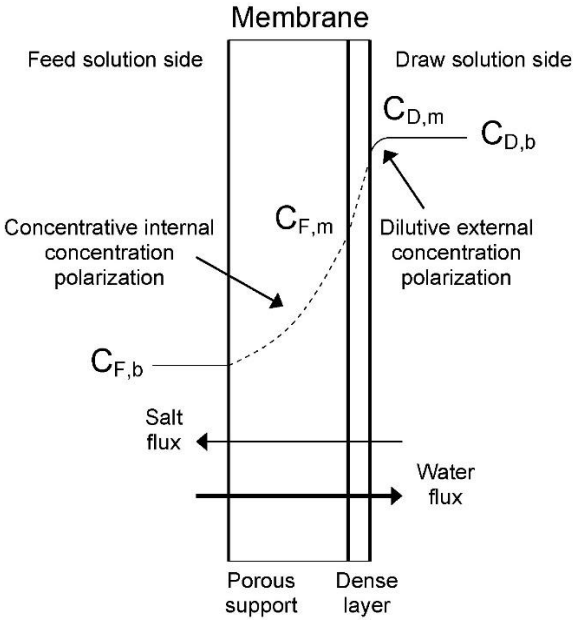

Figure 2: Imperfect Membrane allowing both water and reverse salt flux. Reprinted with permission from Achilli et al. [10]. Copyright 2009 Elsevier

$$J_s = B(C_{D,m} - C_{F,m}) \quad (10)$$

where J_s(mol/(m^2.h) is the salt flux, $C_{D,m}, C_{F,m}$ (mol/L) are the concentration of draw and feed at the active layer of the membrane respectively.

This reverse salt flux leads to performance limitation in both the active and support layers of the membrane. As water permeates through the membrane from the feed to the draw side, salt particles are engrained in the semipermeable active layer and also accumulate in the support layer of the membrane. In this way, the concentration at the porous support layer $C_{F,m}$ is higher when compared to the bulk feed concentration $C_{F,b}$. On the draw side, the concentration just at the surface of the membrane $C_{D,m}$ is less than the concentration of the bulk draw solution $C_{D,b}$. The concentrations just at the membrane surface can be expressed in terms of the bulk concentration by the equations (11) and (12)

$$C_{D,m} = C_{D,b}\, exp\left(-\frac{J_w}{k}\right) + \frac{B}{J_w}\left(C_{D,m} - C_{F,m}\right)\left[1 - exp\left(-\frac{J_w}{D}\right)\right] \tag{11}$$

$$C_{F,m} = C_{F,b}\, exp\left(\frac{J_w S}{D}\right) + \frac{B}{J_w}\left(C_{D,m} - C_{F,m}\right)\left[exp\left(\frac{J_w S}{D}\right) - 1\right] \tag{12}$$

where $C_{D,b}$ and $C_{F,b}$ are the concentration (mol/L) of the draw and feed in the bulk solution respectively.

Substituting equations (11) and (12) into (10), the full expression of the reverse salt flux is;

$$J_s = B\left[\frac{C_{D,b}\, exp\left(-\frac{J_w}{k}\right) - C_{F,b}\, exp\left(\frac{J_w S}{D}\right)}{1 + \frac{B}{J_w}\left[exp\left(\frac{J_w S}{D}\right) - exp\left(\frac{J_w}{k}\right)\right]}\right] \tag{13}$$

To get the water permeate flowrate $\dot{V}_P$ (L/hr) across the membrane, the water flux J_w is integrated over the total area A_m of the membrane;

$$\dot{V}_P = \int_0^{A_m} J_w\, da \tag{14}$$

The molar flowrate can in turn be gotten by using the molar volume gotten from the Q-electrolattice EoS to convert the volumetric flowrate.

The salt molar flowrate (mol/s) can be gotten by integrating the salt flux J_s over the area of the membrane;

$$\dot{m}_{P,s} = \int_0^{A_m} J_s \, da \tag{15}$$

Both water and salt fluxes depend on the concentration and osmotic pressure which in turn depends on the flux profile at the membrane surface. This makes analytical integration difficult and a numerical technique is used instead to estimate the concentration profile in the membrane unit. The mass transfer equations are solved for each discrete element of the membrane and the boundary conditions are determined by the feed and draw inlet streams using sufficient step size.

Assuming that the membrane operates isothermally and that pressure drop across the membrane unit is user-specified, for each element j, the following mass balances must be satisfied;

$$n_{w,j-1}^{D} + \frac{\int_0^{A_m} J_w \, da}{V_m * 3600 * 1000} = n_{w,j}^{D} \tag{16}$$

$$n_{s,j-1}^{D} - \frac{\int_0^{A_m} J_s \, da}{3600} = n_{s,j}^{D} \tag{17}$$

$$n_{w,j-1}^{F} - \frac{\int_0^{A_m} J_w \, da}{V_m * 3600 * 1000} = n_{w,j}^{F} \tag{18}$$

$$n_{s,j-1}^{F} + \frac{\int_0^{A_m} J_s \, da}{3600} = n_{s,j}^{F} \tag{19}$$

where n^D and n^F (mol/s) are the draw and feed molar flowrates, respectively, J_w is the water permeability (L/(m^2.h)), J_s is the salt flux (mol/(m^2.h)), A_m is the membrane area (m^2), V_m is the molar volume of the solution (m^3/mol). The molar volume is calculated by the EoS at the solution's pressure and temperature. The subscripts s and w represent solute and water in the draw and feed streams and the superscripts D and F represent draw and feed respectively.

For a full-scale membrane, the power density is given by;

$$\frac{\dot{W}}{A_m} = \dot{W}_{pump} + \dot{W}_{turbine} \tag{20}$$

where $\dot{W}_{pump}$ and $\dot{W}_{turbine}$ are the shaft power of the pump and turbine respectively.

2.4 COST ESTIMATION METHODS

Plant costing can be predicted using various design philosophies when the actual cost of equipment from the vendor is not available at the time of costing. If previous cost data is available, Turton et al. [35] estimated that the relationship between the purchased costs and an attribute that relates to the capacity of the equipment is given by

$$\frac{C_a}{C_b} = \left(\frac{A_a}{A_b}\right)^n \tag{21}$$

where A is the equipment cost attribute (such as the power of a pump), C is the purchased costs and n is the cost exponent. Subscript a refers to the equipment with the required attribute and b refers to the equipment with the base attribute (e.g. for a pump, the cost corresponding to a base power output is known). This exponent 'n' varies for different equipment and is a

representation of the advantage of economy of scale and is usually taken as 0.6 or 0.7 for process equipment [36].

To correct for inflation thus bringing costs of the same equipment from different years to a current time, the relationship is given as

$$C_2 = C_1\left(\frac{I_2}{I_1}\right) \tag{22}$$

where C is purchased cost, I represents the cost index, subscript 2 represents the current time and 1 represents the base time.

There are three main cost indices used to correct for inflation in chemical engineering plants - The Nelson-Farrar Refinery Index, The Marshall and Swift (M&S) Index, and the Chemical Engineering Plant Cost Index (CEPCI) [37]. CEPCI is used in this work.

To calculate total capital costs, there are some methods proposed in literature;

2.4.1 LANG FACTOR TECHNIQUE

This method gives an order-of-magnitude estimate and gives the total cost of a plant by multiplying the sum of basic equipment cost by a Lang factor [38].

$$C_n = F_{Lang}\sum_{i=1}^{n} C_{p,i} \tag{23}$$

where C_n is the capital cost of the plant, F_{Lang} is the Lang factor (gotten from Lang tables) and it varies depending on the type of plant, n is the total number of units and $C_{p,i}$ is the purchased cost of each equipment unit.

2.4.2 UNIT COST ESTIMATE

This cost estimation method is useful in cases where past data exists for executed projects. It takes into cognizance costs ranging from labor costs for equipment installation to design costs as shown in the cost equation (24) below [39].

$$C_n = \left[\sum_{i=1}^{m} \left(E_i + E_{L,i}\right) + \sum_{j=1}^{a} \left(f_j M_j + g_j M_L'\right) + \sum_{k=1}^{b} f_k H_k + \sum_{l=1}^{c} f_l d_l \right] f_F \tag{24}$$

where C_n is new capital investment, m is the total number of equipment purchased, a is the number of specific materials which is not a piece of equipment (such as pipes), b is the total number of engineering hours, c is the total number of drawings needed to design the plant, E_i is the purchased equipment cost, $E_{L,i}$ is purchased equipment labor cost, f_j is specific material unit cost (j can represent pipe, fitting, elbows, etc.), M_j is the quantity of material in comparable units (j can represent pipe etc.), g_j is the labor cost per employee hour, M_L' is total employee hour for the specified material, f_k is the unit cost for engineering, H_k is the engineering employee hour, f_l is unit cost per drawing/specification, d_l is the number of drawings/specifications, f_F is the construction factor which is always greater than one and gives a margin to account for uncertainties.

2.4.3 PERCENTAGE OF DELIVERED EQUIPMENT COST

In this method, after the determination of fixed equipment costs, other costs that go into the setup and commissioning of the plant are calculated based on a percentage of the delivered equipment costs [39].

$$C_n = \left[\sum_{i=1}^{m} E_i \ \left(1 + f_{1,i} + f_{2,i} + f_{3,i} + \cdots\right) \right] f_l \tag{25}$$

where E is the cost of the major equipment delivered (e.g., pump) and f_1, f_2 are multiplying factors for piping, electrical, instrumentations, needed to install the main equipment, subscript i, represents the particular equipment of interest (e.g. pump, turbine) and f_I is the indirect cost factor which is always greater than one.

2.4.4 MODULE COSTING METHOD

This costing method includes the free-on-board costs (F.o.B.), the costs of materials needed for installation, and the indirect costs that add to the engineering expenses [35].

$$C_{BM} = C_P^0 F_{BM} \tag{26}$$

where C_{BM} is the bare module equipment cost, C_P^0 is the cost of equipment at base conditions, F_{BM} is the cost factor from tables by Turton et al. [35] and it is based on the operating pressure and the material of construction.

To allow for cost consideration due to a different type of material being used for high-pressure operations, the equation is modified as shown below and correlation constants B_1 and B_2 are found in tables provided by Turton et al. [35].

$$C_{BM} = C_p^0 F_{BM} = C_p^0 (B_1 + B_2 F_M F_P) \tag{27}$$

where B_1 and B_2 are material-specific and can be found in tables [35], F_M is the material of construction factors which is not equal to one for any material that is not carbon steel and F_P which is the pressure factor that shows increased costs for high-pressure operations.

2.5 COST ESTIMATION SCHEMES

Reverse Osmosis has had a head start on PRO and, due to some similarities in mechanical equipment, some ideas on costing have been borrowed from the literature on costing reverse osmosis (RO) plants. In desalination plants, there are four schemes of desalination cost

estimates [40]. They are Conceptual, Preliminary, Budgetary, and Detailed. Each of these estimates has different levels of accuracy

2.5.1 CONCEPTUAL COST ESTIMATE

This cost modeling is performed as a means to compare between supply alternatives without knowledge of the full scope of the project. For this type of costing, its strength is based on knowledge of similar projects already executed which are used as benchmarks to which incremental "plus" or "minus" cost factors are applied. This gives rise to the name 'incremental budgeting' [40] and it is a fatal flaw analysis of the project. The accuracy deviation is in the range of -50 – 100%.

2.5.2 PRELIMINARY COST ESTIMATE

This type of costing defines a basis for further analysis. It represents the cost estimate of the plant without going into location-specific details such as cost of land and transportation, or country-specific labor costs [40]. This costing type combines the use of costing models or quotes from suppliers with knowledge of specific processes to make a judgment on costs. The accuracy deviation is in the range of -30 to +50%. This is the type of cost estimation carried out in this work.

2.5.3 BUDGETARY COST ESTIMATE

This type of costing is done during authorization for project implementation. It takes preliminary costings and adds land use considerations such as geotechnical surveys, architectural designs as well as costs of supply systems logistics to the plant. [40]. It accounts for site-specific factors. The accuracy deviation is in the range of -15 to +30%.

2.5.4 DETAILED COST ESTIMATE

This cost estimate determines the tender/bidding price for a project. It goes beyond the Budgetary cost estimate to include contractor profit margin, binding vendor supply prices, costs

for startup and commissioning, and costs due to governmental regulation [40]. It is a highly accurate estimation method with an accuracy deviation in the range of -5 to +10%.

3 METHODOLOGY

To achieve the goal of investigating the techno-economic feasibility of PRO to produce energy, the capabilities of the simulator were extended to handle the economic calculations of a full scale plant.

Models are used to evaluate the costs of each component that makes up the PRO system as shown in Figure 3 and the Chemical Engineering Plant Cost Index (CEPCI) is used to correct for inflation. A typical PRO process has 5 modules as described below:

1. the semipermeable membrane, which selectively allows water (but not salt, ideally) molecules to permeate through it;
2. the booster pump (or high-pressure pump), which drives the draw solution (high salinity stream) to the membrane;
3. the feed pump (or low-pressure pump), which drives the feed (low salinity stream) to the membrane. This is the stream that permeates through the membrane;
4. the pressure exchanger, which receives part of the pressurized stream with the diluted draw solution that exits the membrane unit. Its purpose is to reduce the pumping requirement of the booster pump;
5. the hydro turbine where energy is recovered from the other part of the pressurized stream with the diluted draw solution that exits the membrane unit.

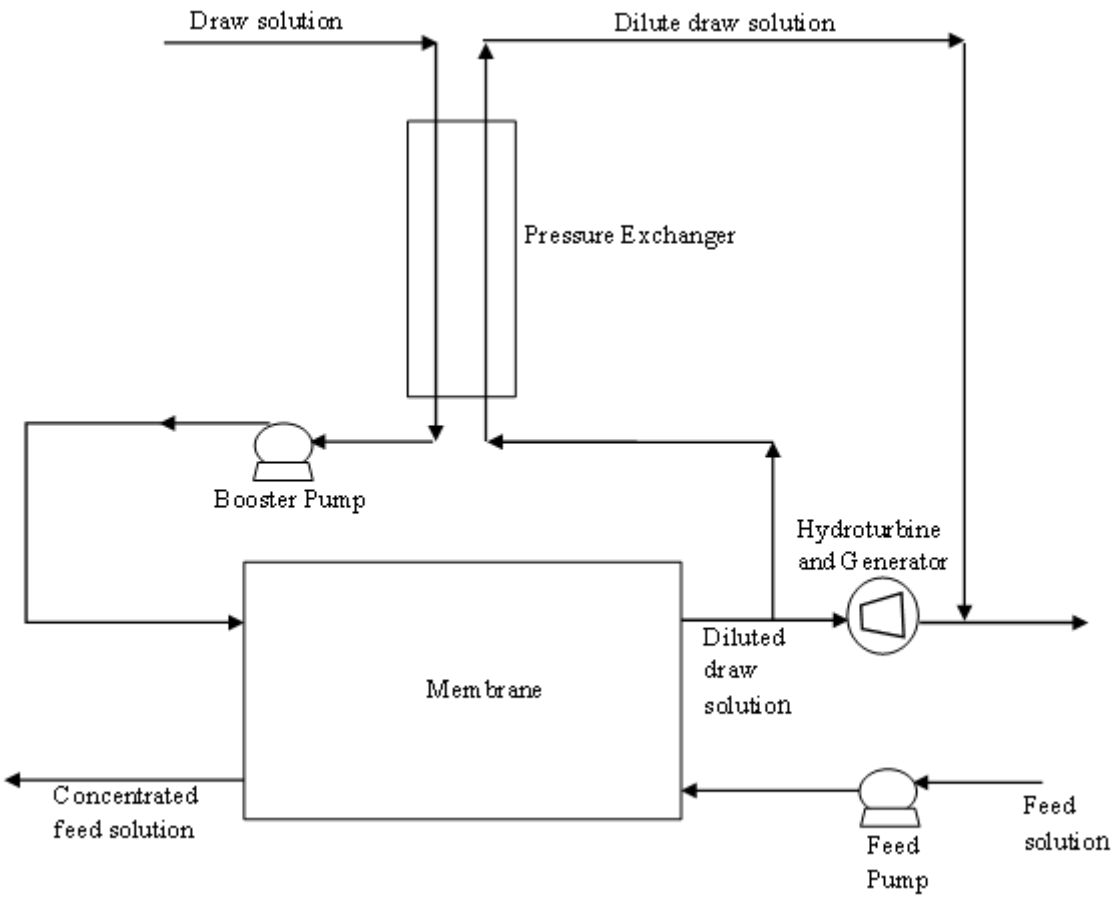

Figure 3: Typical PRO configuration. Figure adapted from Manzoor [33]

The following sections show the breakdown of the CAPEX and OPEX computation.

3.1 CAPITAL COSTS (CAPEX)

The evaluation of capital costs is based on empirical cost correlations that depend on a few technical parameters that are characteristic of each type of equipment. For example, the cost correlations for pumps and turbines often are explicit functions of mechanical power; the cost correlations for vessels generally depend on the vessel's volume and operating pressure. This section presents the main equations of the models that are used to determine the design parameters of PRO process components and the corresponding cost correlation formulas for these components. The models are developed and applied under the assumption that the PRO process is continuous and operates at steady-state. The capital cost correlations provide

estimates in U.S. dollars in a given year. The obtained costs are updated using the Chemical Engineering Plant Cost Index (CEPCI) [41].

3.1.1 PUMP AND TURBINE MODULES

3.1.1.1 Design Equation

The cost of pumps and turbines depends on power. The pump is modeled based on the first and second laws of thermodynamics for an open system. The equation, as shown in equation (28) is the energy balance obtained by assuming that the pump is adiabatic, operates at steady-state, and that changes to the fluid's kinetic and potential energies are negligible:

$$\dot{W}_{shaft} = \dot{n}[h_{out}(T_{out}, P_{out}, x_{out}) - h_{in}(T_{in}, P_{in}, x_{in})] \tag{28}$$

where h represents molar enthalpy, x represents an array with the mole fraction of all components, $\dot{n}$ represents the molar flowrate, T and P represent temperature and pressure, respectively, and the subscripts in and out correspond to stream properties of the inlet and outlet. It is assumed that the molar flow rate and the component mole fractions remain unchanged across the pumps. To calculate the temperature of the outlet stream, T_{out}, and for a specified outlet pressure, assuming isentropic conditions enables the first approximation of the outlet temperature, by solving:

$$\dot{n}[s_{out}(T_{out}, P_{out}, x_{out}) - s_{in}(T_{in}, P_{in}, x_{in})] = 0 \tag{29}$$

where s represents the molar entropy

The reversible and adiabatic shaft power, $\dot{W}_{shaft,rev}$, can be calculated by substituting the evaluated temperature into the equation (28). The reversibility assumption is relaxed such that when the efficiency (η) of the mechanical component is specified, the actual power can be calculated.

$$\dot{W}_{shaft} = \frac{\dot{W}_{shaft,rev}}{\eta_{pump}} \tag{30}$$

An analogous procedure is executed for the turbine, with

$$\dot{W}_{shaft} = \dot{W}_{shaft,rev} * \eta_{turbine} \tag{31}$$

The outlet stream temperature, T_{out}, is then re-evaluated such that it satisfies the energy balance, equation (28).

3.1.1.2 Cost Equation

The models to calculate the cost relationship for the pumps and turbines are obtained from Feinberg [42]. The correlations were developed using cost information from suppliers in the year 2014 and the CEPCI inflation index for that year was 576.1. The cost correlation for pumps is:

$$CC_{pump} = \quad 0.4744\dot{W}_{pump}^2 + 606.76\dot{W}_{pump} + 663998 \qquad \dot{W}_{pump} > \ 550kW \tag{32}$$

$$CC_{pump} = -0.617\dot{W}_{pump}^2 + 1576.58\dot{W}_{pump} + 350323 \qquad 350kW < \dot{W}_{pump} < 550kW \tag{33}$$

$$CC_{pump} = \quad -1.7084\dot{W}_{pump}^2 + 2546.4\dot{W}_{pump} + 36648 \qquad \dot{W}_{pump} < 350kW \tag{34}$$

The cost correlation for turbines is:

$$CC_{\text{turbine}} = 0.0009\dot{W}_{\text{turbine}}^2 + 204.9\dot{W}_{\text{turbine}} + 127049 \tag{35}$$

where $\dot{W}_{pump}$ and $\dot{W}_{turbine}$ is the power of the pump and turbine, respectively, in kW.

3.1.2 PRESSURE EXCHANGER

3.1.2.1 Design Equation

A pressure exchanger has two sides – a pressurization side and a depressurization side. It operates on the mechanical energy supplied by the high-pressure flow which is transferred to the low-pressure flow. Mechanical power from the depressurization side is transferred to the pressurization side and thus, the pressurization side is similar to a pump. The depressurization side is similar to a turbine. By assuming adiabatic and reversible operations, the isentropic power ($\dot{W}_{HP,rev}$) and temperature can be calculated using equations (28)and (29) while the actual power transferred from the depressurization side ($\dot{W}_{HP}$) is evaluated by substituting equation (31) into (28) to allow re-evaluation of the outlet temperature needed to satisfy the energy balance.

The output pressure of the depressurization side is unknown but can be calculated from the power supplied by the pressurization side ($\dot{W}_{HP}$) after accounting for frictional losses calculated as $(1-\eta_{LP})\dot{W}_{HP}$. The entropy balance for the pressurization side is given as;

$$\dot{n}_{LP}\left(s_{LP,in}-s_{LP,out}\right)+\dot{S}_{gen}=0 \tag{36}$$

where $\dot{n}_{LP}$ is the molar flow rate of the low-pressure stream and $\dot{S}_{gen}$ is the rate of entropy generation given as;

$$\dot{S}_{gen}=\frac{(1-\eta_{LP})\dot{W}_{HP}}{T} \tag{37}$$

where T is the arithmetic average temperature of the inlet and outlet stream of the pressurization side. The energy and entropy balance for a pressure exchanger pressurization side is shown in equations (38) and (39) such that solving both simultaneously give the values of $T_{LP,out}$ and $P_{LP,out}$.

$$\dot{n}_{LP} h\left(T_{LP,out}, P_{LP,out}, x_{LP}\right) = \dot{n}_{LP} h\left(T_{LP,in}, P_{LP,in}, x_{LP}\right) + |\dot{W}_{HP}| \quad (38)$$

$$\dot{n}_{LP}\, s\left(T_{LP,out}, P_{LP,out}, x_{LP}\right) = \dot{n}_{LP}\, s\left(T_{LP,in}, P_{LP,in}, x_{LP}\right) + \frac{(1-\eta_{LP}) \times |\dot{W}_{HP}|}{\frac{T_{LP,in}+T_{LP,out}}{2}} \quad (39)$$

where $\dot{n}$ represents molar flowrate, h represents molar enthalpy, x represents component mole fraction, LP represents the low-pressure stream, η_{LP} represents the efficiency of the low-pressure stream and $\dot{W}_{HP}$ is power transferred from the depressurization side of the pressure exchanger.

3.1.2.2 Cost Equation

The costing model of a pressure exchanger depends on the volumetric flow rate through it. The cost model for pressure exchanger is based on cost correlation from Energy Recovery International (ERI) as reported in [43] with $\dot{V}_{PX}$in m^3/h. The model was developed in 2006 and the CEPCI inflation index was 499.6.

$$CC_{PX} = 19802.4\ (\dot{V}_{PX})^{0.58} \quad (40)$$

3.1.3 MEMBRANE

The membranes do not have costing models but costs depend on the required membrane area, the manufacturer, and the type of membrane. The costs of membrane can range from \$ -14.18/m^2 [44] to \$25/m^2 [23]. \$15/m^2 was used as the membrane cost in this work.

3.1.4 PRESSURE VESSEL

The pressure vessel houses the spiral wound membranes. The cost model is obtained from Sim et al. [45]. The cost depends on the number of pressure vessels needed (N_{PV}), which in turn depends on the area of membrane to be housed. In general, in desalination processes, there are typically 7 membrane elements per pressure vessel and each membrane element has an area of

40.88m^2 [44]. The model was developed in 2013 and the CEPCI inflation index for that year was 567.3

3.2 OPERATING COSTS (OPEX)

The main operating costs encountered in desalination plants are energy (power), maintenance, chemicals, labor, and membrane replacement [46]. However, for PRO plants, operating costs computations reduce to maintenance, chemicals and pretreatment, labor, and membrane replacement since it generates power.

3.2.1 PRETREATMENT

Pretreatment is done to prevent membrane fouling which occurs when particles accumulate on the surface or in the membrane pores [47]. The energetic cost of pretreatment is assumed to range between 0.1 – 0.4 kWh/m^3 [48].

$$OC_{Pretreat} = 0.256\frac{kWh}{m^3} * \ C_{electricity}\frac{\$}{kWh} * \left(\dot{V}_{draw} + \dot{V}_{feed}\right) * \frac{m^3}{s}\ x\ 3.154e07\frac{s}{yr} \qquad (41)$$

$C_{electricity}$ is taken as \$0.032/kWh, which is the year 2021 electricity cost in Qatar. The value of $0.256kWh/m^3$ is an approximation of the energetic cost of pretreatment as reported by Straub et al. [48]

3.2.2 CHEMICALS

The annual cost of chemicals depends on the sum of the flowrates of feed and draw treated. An inherent assumption to this is that both feed and draw require the same type of treatment. This simplifying assumption may not be true in all cases depending on the composition of the feed and draw.

The annual cost of chemicals (\$/m^3) ranges from \$ 0.018/m^3 in year 2008 [49] to a bracket between 0.03 – 0.06\$/m^3 in year 2018 [46].

$$OC_{chem} = \left(\dot{V}_{draw} + \dot{V}_{feed}\right)\frac{m^3}{s} * 24\frac{hrs}{day} * 365\ \frac{days}{yr} * C_{unit}\frac{\$}{m^3} \quad (42)$$

where C_{chem} is the total annual cost of chemicals, $\dot{V}_{draw} + \dot{V}_{feed}$ is the total flow rate in m^3/hr. of liquid (draw and feed) to be treated and C_{unit} is the unit cost of chemicals in \$/m^3.

3.2.3 MEMBRANE REPLACEMENT

Reverse osmosis membranes usually have a life span between 5 and 7 years [50] or 3 and 5 years [51] and the plants last for an average lifetime of about 20 years [23]. Based on this information, the operating cost associated with membrane replacement is [23];

$$OC_{mr} = \frac{\left(\$_{mem} * A_m * \left(\frac{plant\ life}{membrane\ life} - 1\right)\right)}{Plant\ life} \quad (43)$$

where OC_{mr} is the cost of membrane replacement per year, $\$_{\mathrm{mem}}$ is the purchasing cost of the membrane per unit area, A_m is the total area of the membrane to be replaced. For this work, a membrane life of 5 years is used.

3.2.4 LABOR AND MAINTENANCE

Labor costs largely depend on the location and size of the plant, while maintenance costs depend on the size of the plant. A simple approximation takes these costs (annual amount) as a percentage of the capital cost of the plant [23].

Together, they are taken as 3% of initial capital costs [23]. This equals the amount that would be spent yearly on labor and maintenance

3.3 ECONOMIC EVALUATION AND DECISION MAKING – LEVELIZED COST OF ELECTRICITY (LCOE)

A parameter that combines both economic and energetic information of energy generation systems is the LCOE, which is calculated using the formula as shown below [5];

$$LCOE = \frac{\left(C_{CAPEX} + C_{OPEX}\,\frac{(1+i)^N - 1}{(1+i)^N * i}\right)}{E\,\frac{(1+i)^N - 1}{(1+i)^N * i}} \tag{44}$$

where C_{CAPEX} is the capital expenditure, C_{OPEX} represent annual operating costs, i represents the yearly discounting factor, N represents the total life of the plant in years and E represents the net total electricity produced by the plant every year (kWh/yr.) A graphical representation of the LCOE is shown in Figure 4 below;

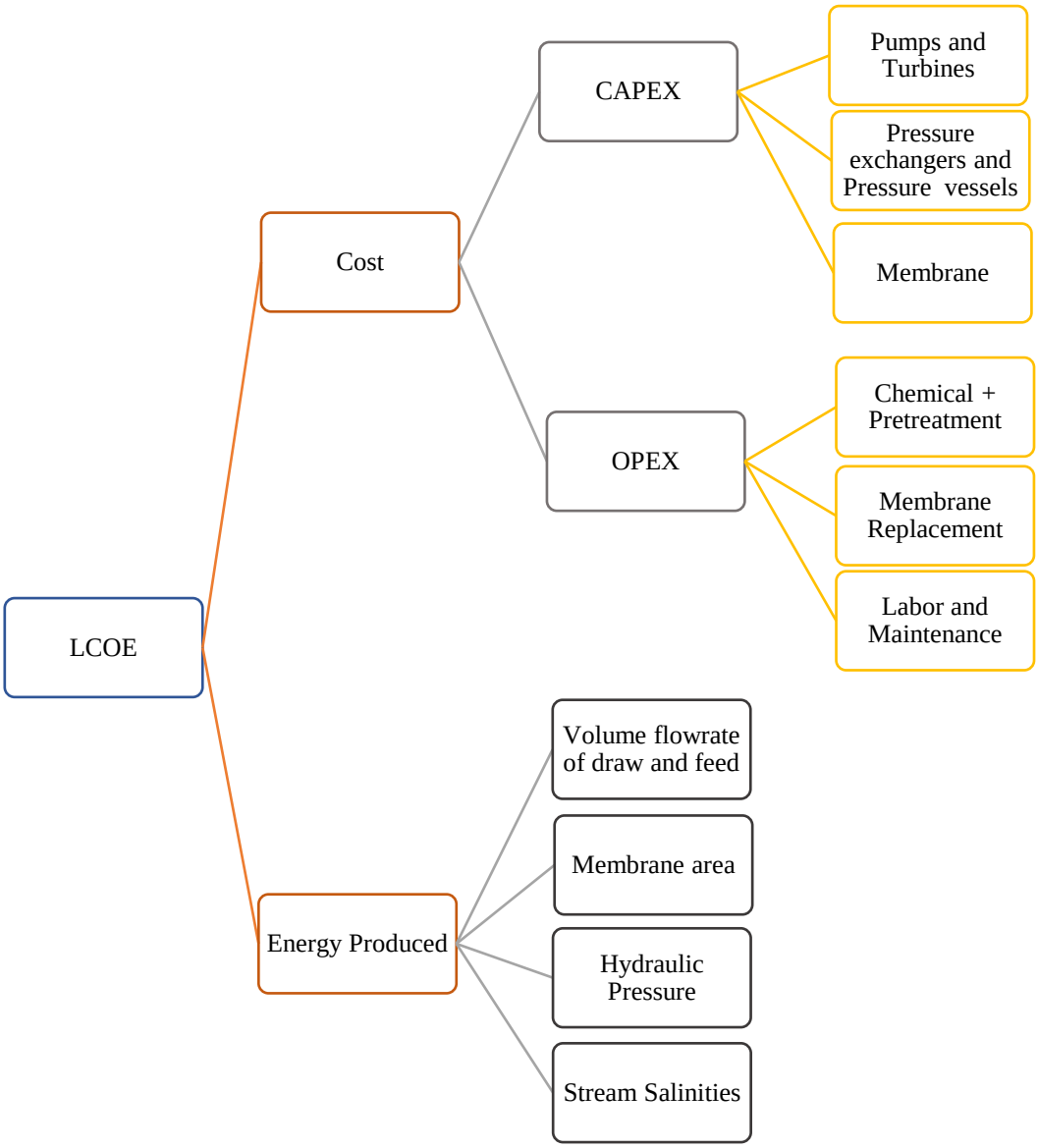

Figure 4: Components of the LCOE for a PRO Plant

In general, the LCOE is used to compare amongst different types of electricity generation technologies. The LCOE depends on the cost of generation as well as the amount of electricity generated. For a PRO plant, the cost of generation is made up of capital and operating expenditure. The capital expenditure (CAPEX) is the sum of the costs of the mechanical equipment and membrane used in power generation. The OPEX refers to the costs for labor and maintenance, membrane replacement, chemicals, and pretreatment. The energy produced

is a function of the draw and feed flowrates and salinity, membrane properties such as water and salt permeability as well as the applied hydraulic pressure.

Figure 5 presents the flowchart that shows the work flow within the simulator.

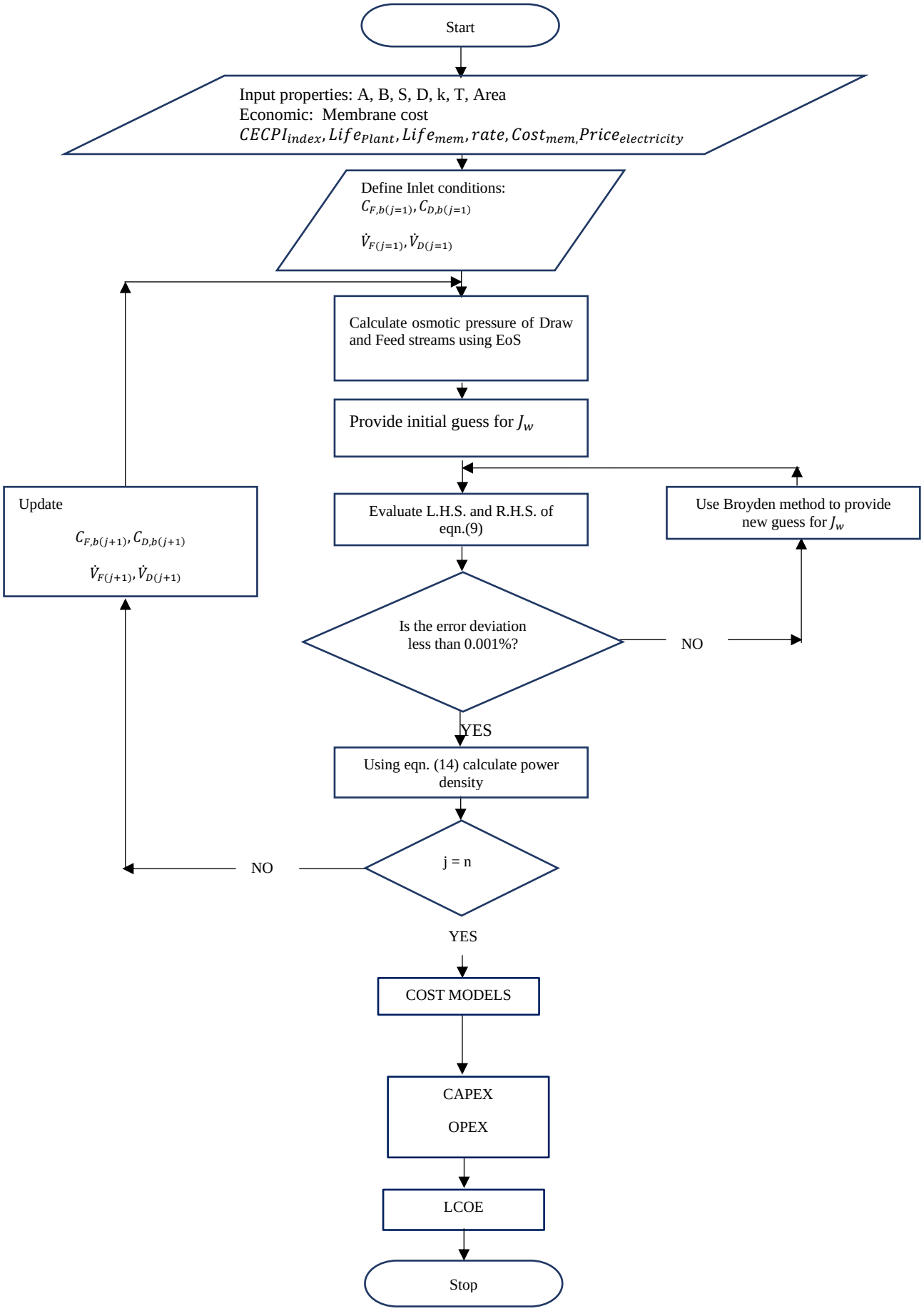

Figure 5: Flowchart showing simulator workflow

4 RESULTS

The developed PRO simulator had its capabilities extended to perform techno-economic analysis. Using the DAKOTA Sensitivity Analysis and Optimization tool [52], various analyses were carried out to understand system behavior in the face of both technical and economic constraints.

4.1 ENERGETIC AND ECONOMIC OPTIMUM OCCUR AT DIFFERENT SYSTEM CONDITIONS

To arrive at this result – that energetic and economic optimum occur at different system conditions – a sensitivity analysis was carried out using membrane sizes ranging from 20,000 to 200,000 m^2 and hydraulic pressure ranging from 10 to 100 bar. Flowrates of the draw and feed were scaled up in tandem with membrane sizes for each analysis.

The results reported in Figure 6 and Figure 7 are for 20,000 and 200,000m^2 membrane area respectively at equal volumetric flowrates of the draw and feed such that ($\phi = 0.5$) where;

$$\phi = \frac{\dot{V}_{feed}}{\dot{V}_{draw} + \dot{V}_{feed}}$$

For each area, the curves shown are for Net Power produced and LCOE at various values of pressure. The net power of the system can be defined as;

$$\dot{W}_{system} = \dot{W}_{turbine} - \dot{W}_{pump}$$

At both membrane areas and specified process conditions, the pressure that maximizes the net power produced and the pressure that minimizes the LCOE occurs at different operating conditions of the system. It has been established from literature that for an ideal membrane and using dilute solutions, the theoretical optimum applied pressure, which is the pressure at which power density is maximum, is at half the osmotic pressure difference [53][23]. However, for

full scale membranes, the actual optimum differs from half of osmotic pressure difference due changes in the driving force along the membrane. This change in driving force is due to concentration polarization of the membrane at the feed stream side and the dilution of the draw stream [33][54].

Recent studies have reported that this value may be around 40% - 47% [54] but the LCOE occurs at pressures lower than 40% of the osmotic pressure difference – which is the least percentage currently reported in literature.

At 20,000m^2 and at the process conditions specified in Table 2, the pressure that maximizes net power produced is at 79 bar. This is hypothetical case because the maximum pressures that current PRO membranes can withstand are much less than this value. In contrast to this, the pressure that minimizes the LCOE is 55 bar. While increased power production is desirable, the cost of generation is such that, beyond a certain point, the additional power produced does not justify the costs of production.

The effect of the trade-off between cost of generation and power production is even more dramatic at higher areas. At 200,000m^2, the pressure that minimizes LCOE is 25 bar. While larger areas correspond to higher power generation, the combined effect of the increased cost of pumping the required draw solution through the system, and the higher cost of the membrane due its area make operating the system in maximum power production mode undesirable.

Table 2: Properties and Process conditions used in simulation. Membrane used is HTI-CTA reported by Straub et al.[55]

Property	Values	
Area (m^2)	20,000	200,000
Volumetric flowrate draw (m3/s)	0.252	2.52
Volumetric flowrate feed (m3/s)	0.252	2.52
Water Permeability (L/m^2.h.bar)	2.49	
Salt permeability (L/m^2.h)	0.39	

Table 2: Properties and Process conditions used in simulation. Membrane used is HTI-CTA reported by Straub et al.[55] (continued)

Property	Values	
Structural parameter (m)	$5.64x10^{-4}$	
Diffusion coefficient (m^2/s)	$1.48x10^{-9}$	
Mass transfer coefficient ($L/m^2.h$)	99.0	
Hydraulic pressure (bar)	{10 – 100}	
Salinity	Draw salinity	Feed salinity
Temperature	298.15	298.15
Na^+ ion (g/L)	68.97	0
Cl^- ion (g/L)	106.51	0

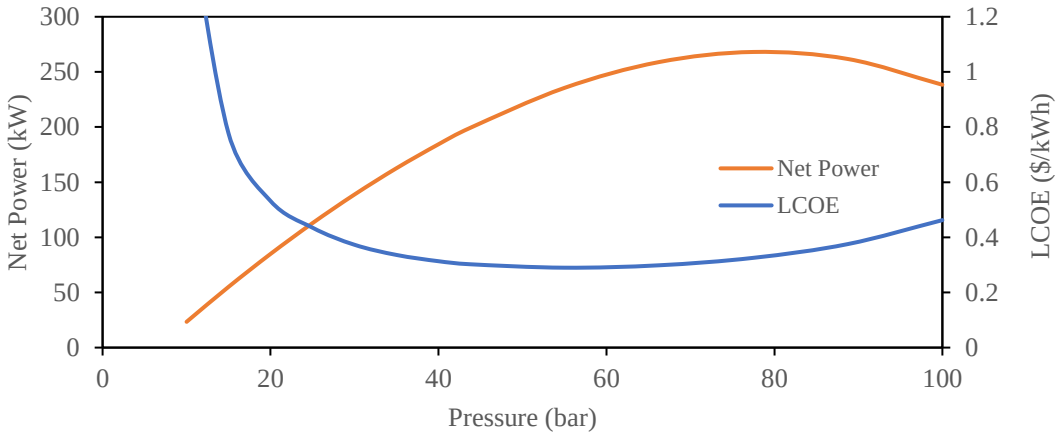

Figure 6: Net Power and LCOE vs Pressure at 20,000m^2 membrane area. Analysis done at ϕ =0.5

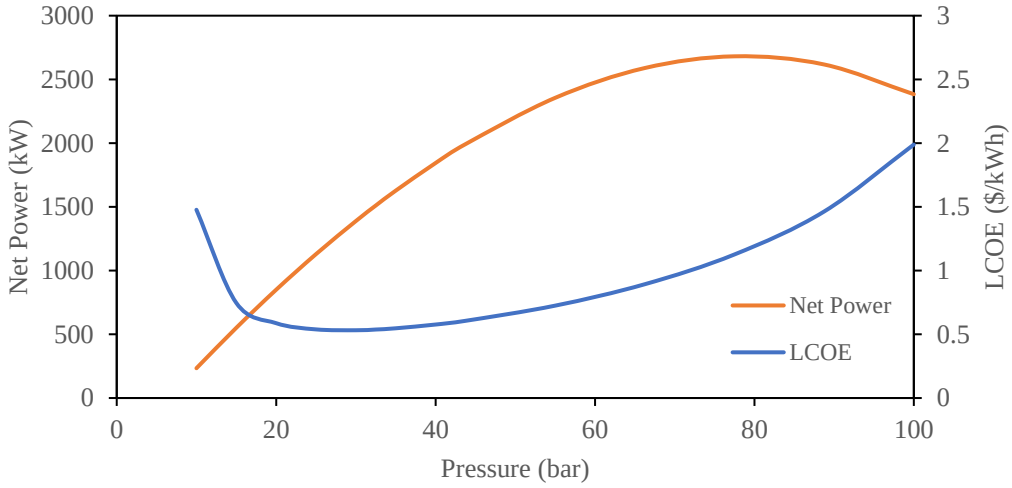

Figure 7: Net Power and LCOE vs Pressure at 200,000m2 membrane area. Analysis done at ϕ=0.5

4.2 OPTIMAL ECONOMICAL OPERATING PRESSURE RANGE DECREASES AS PLANT SYSTEM SIZE INCREASES

This section shows that there is a narrower range of technical parameter allowance for optimum economic performance as system size increases. Table 3 presents the data used in performing the simulation for this section. The flowrate for the draw is fixed while that of the feed varies such that plot legends in Figure 8 and Figure 9 are presented on the basis of ϕ.

This simulation was done for membrane sizes ranging from 5,000 to 500,000m^2, but the results are shown for 20,000 and 200,000m^2 for ϕ ranging from 0.25 to 0.62. Figure 8 and Figure 9 show results for 20,000m^2 and 200,000m^2 membrane areas respectively.

At 20,000m^2 and for different values of ϕ, the plot of LCOE ($/kWh) against pressure (bar) in Figure 8 shows that, between 43.75 and 66.25 bar, the LCOE reaches a minimum. The percentage change in the value of LCOE between these pressures range from 1.77% at ϕ=0.25 to 4.26% at ϕ=0.63. The changes in LCOE within this pressure range is less than 5% and indicates that the system can operate within this range with little detrimental effect to plant techno-economics. For comparison, the two renewable energy technologies with the least value of LCOE as at 2019 [56] (Hydro and Onshore Wind) have a percentage difference of 11.3% between their values.

However, at 200,00m^2, the range of pressure that minimizes the LCOE is between 21.25 and 33 bar as seen in Figure 9. While we had a band of 22.5 bar (difference between 66.25 and 43.75 bar) to operate within when the system was smaller, this band decreases to 11.75 bar with increased system size. The twin effect of higher pumping costs and higher total membrane costs narrows the range of operating conditions for which LCOE might be minimized.

Table 3:Properties and Process conditions used in Simulation of Operating Pressure Ranges as Area Increases

Property	Values	
Area (m^2)	20,000	200,000
Volumetric flowrate draw (m3/s)	0.25	2.52
Volumetric flowrate feed (m3/s)	{0.084 – 0.75}	{0.84 – 7.58}
Water Permeability ($L/m^2.h.bar$)	2.49	
Salt permeability ($L/m^2.h$)	0.39	
Structural parameter (m)	$5.64x10^{-4}$	
Diffusion coefficient (m^2/s)	$1.48x10^{-9}$	
Mass transfer coefficient ($L/m^2.h$)	99.0	
Hydraulic pressure (bar)	{10 – 100}	
Salinity	Draw salinity	Feed salinity
Temperature	298.15	298.15
Na^+ ion (g/L)	68.97	0
Cl^- ion (g/L)	106.51	0

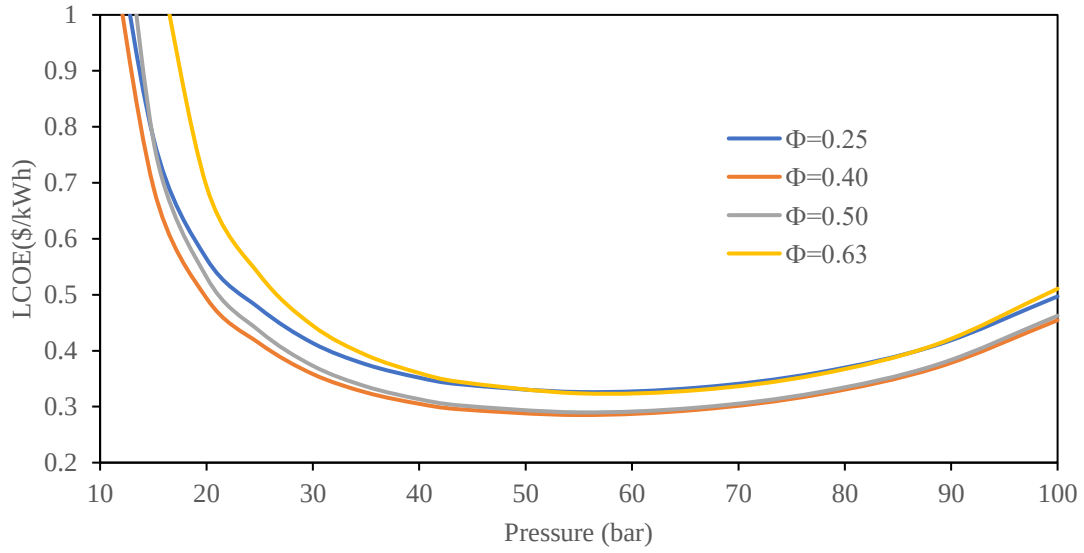

Figure 8: Plot of LCOE vs Pressure at 20,000m^2

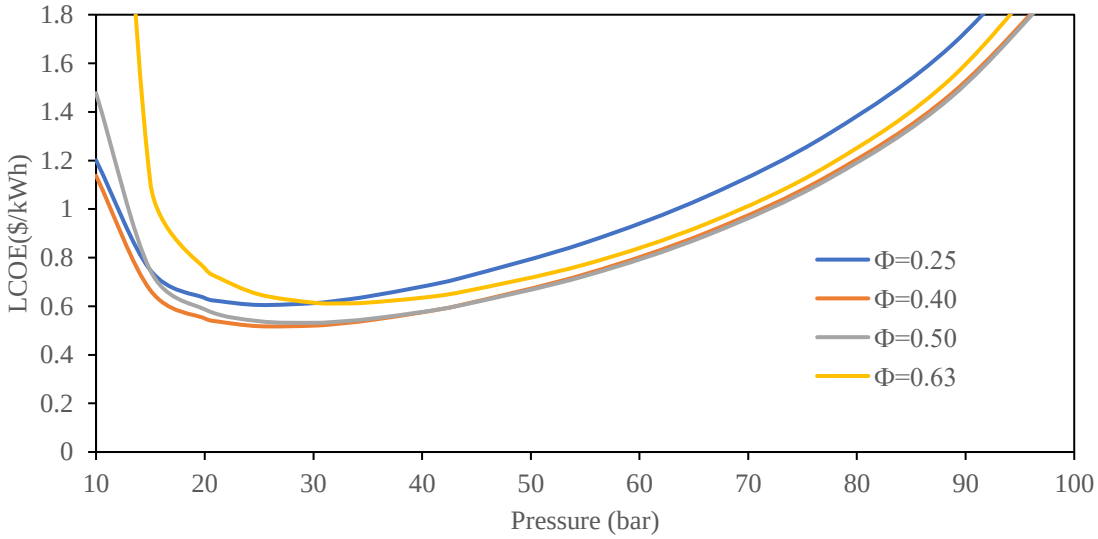

Figure 9: Plot of LCOE vs Pressure at 200,000m^2

4.3 EFFECT OF MEMBRANE PROPERTIES ON LCOE

Membrane properties affect how much power can be produced via PRO for a specific configuration and this, in turn, affects the value of LCOE. An ideal membrane would be one that maximizes flux by increasing the value of water permeability while decreasing salt permeability as much as possible [57].

Although membrane properties such as water permeability (A), salt permeability (B), and structural parameter (S), are usually assumed to be independent of pressure, Madsen et al. [58] have published findings that show that B and S vary with pressure. However, water permeability (A) was reported to be independent of pressure. The results obtained by Madsen et al. for the effect of pressure on the salt permeability and structural parameter were used in the simulator so that these parameters are expressed as functions of applied pressure.

4.3.1 EFFECT OF SALT PERMEABILITY AND MEMBRANE COMPACTION ON LCOE

Madsen et al. [58] report that the variation of salt permeability with pressure can be expressed by a linear relationship defined by an intercept and slope. These values as well as other membrane properties and process conditions that were used in the set-up of the simulator are given in Table 4.

Section 4.3.1.1 reports the analysis made when the intercept of the curve of the salt permeability against pressure is varied and section 4.3.1.2 show results when the slope of the salt permeability against pressure curve is varied.

Table 4: Madsen et al. [14] HTI-CTA membrane properties and Process Conditions

Property	Values	
Area (m^2)	40	
Water Permeability ($L/m^2.h.bar$)	0.42	
	LCOE vs Intercept of B vs P curve	LCOE vs Slope of B vs P curve
Salt permeability(B) ($L/m^2.h$)	{0.0 – 0.75}	0.284
Slope of B vs P line ($L/(m2.h.\ Pa)$)	$8.357x10^{-8}$	$\{2x10^{-9} – 9x10^{-8}\}$
Structural parameter(S) (m)	$1.00x10^{-3}$	
Slope of S vs P line (m/Pa)	$2.367x10^{-10}$	
Diffusion coefficient (m^2/s)	$1.48x10^{-9}$	
Mass transfer coefficient ($L/m^2.h$)	300.0	
Hydraulic pressure (bar)	{10 -90}	
Draw flowrate (m^3/s)	$3.5x10^{-4}$	
Feed flowrate (m^3/s)	$3.5x10^{-4}$	
Temperature	298.15	298.15
Na^+ ion (g/L)	68.97	0
Cl^- ion (g/L)	106.51	0

4.3.1.1 Effect of Salt Permeability (Intercept) on LCOE

To study the effect of the intercept of the Salt Permeability-Pressure relationship on LCOE, the intercept is varied from 0 – 0.75 L/m^2.h with the rate of increase over the pressure range evaluated kept constant. The graphical representation of the range used in the analysis is shown in Figure 10.

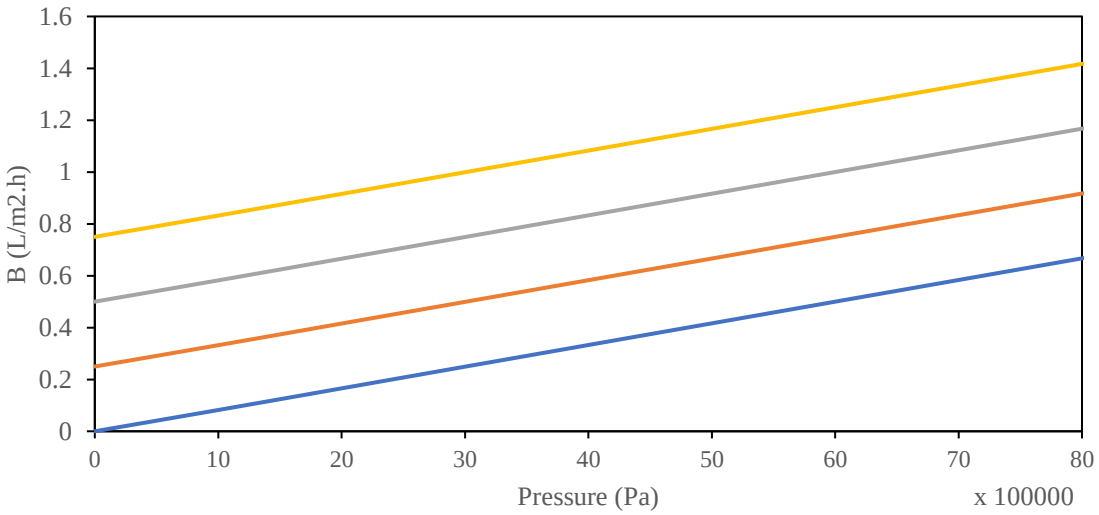

Figure 10: Graphical representation of the variation of intercept with pressure used in problem set-up

.

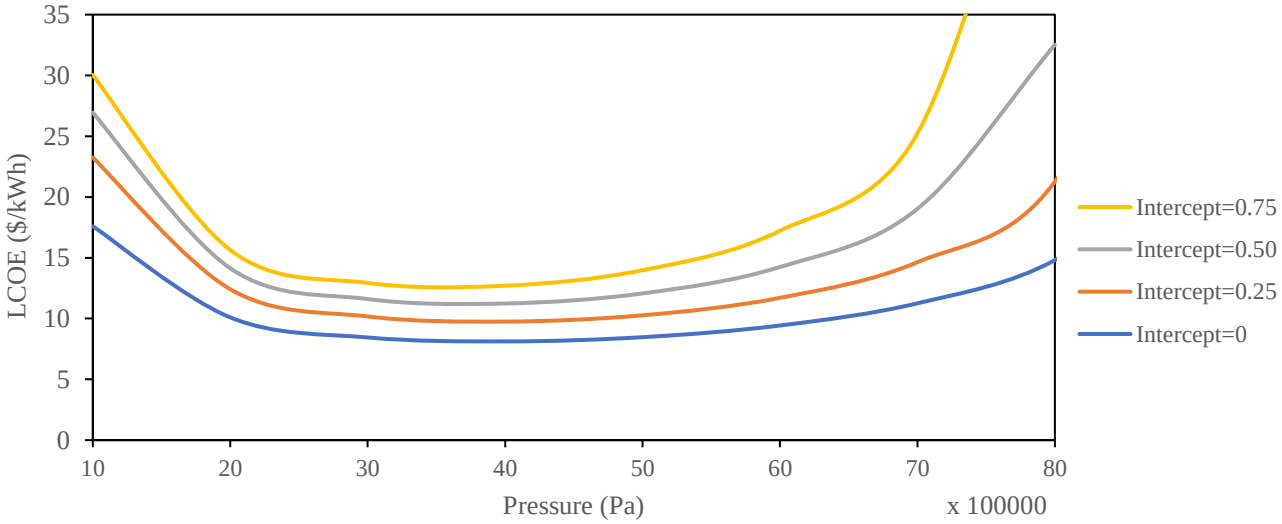

Figure 11: LCOE vs Pressure at different values of B intercept

The result obtained is shown in Figure 11. At any specific pressure, as the value of the intercept increases, the value of LCOE also increases. This is not unexpected because higher values of salt permeability indicate that the membrane is more susceptible to reverse salt flux and thus power produced is lower for the same economic costs. At any specific value of intercept, the LCOE reaches a minimum but increases beyond a certain pressure. This is because, beyond optimal pressure where maximum power is produced, further increase in pressure actually leads to a decrease in power production. This combined effect of increased pumping cost (due to increased pressure) but decreased power production causes a rise in the value of LCOE. Comparing the curves gotten at 0 and 0.75 $L/m^2.h$, when the pressure is increased from 40bar to 60bar the LCOE increased by 16.15% for the membrane with 0 $L/m^2.h$ and 35.62% for that with 0.75 $L/m^2.h$. Thus, LCOE increases at a faster rate for membranes with higher values of salt permeability.

4.3.1.2 Effect of the Rate of Salt Permeability Increase against Pressure on the LCOE

The value of the salt permeability as a function of pressure for different rate of increase values ranging from $9x10^{-8}$ to $2x10^{-9}$ $L/(m^2.h.\ Pa)$ is shown in Figure 12.

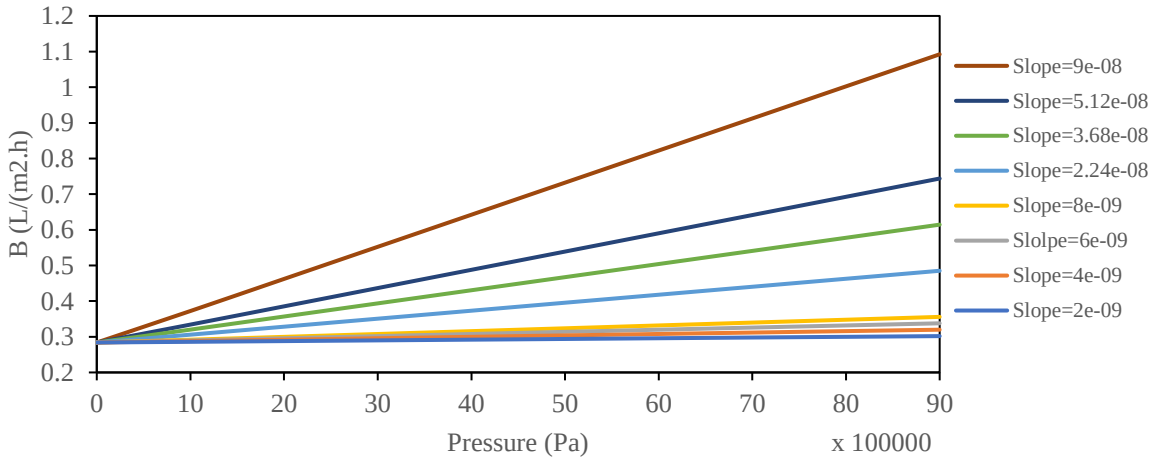

Figure 12: Graphical representation of the variation of slope with pressure used in problem set up.

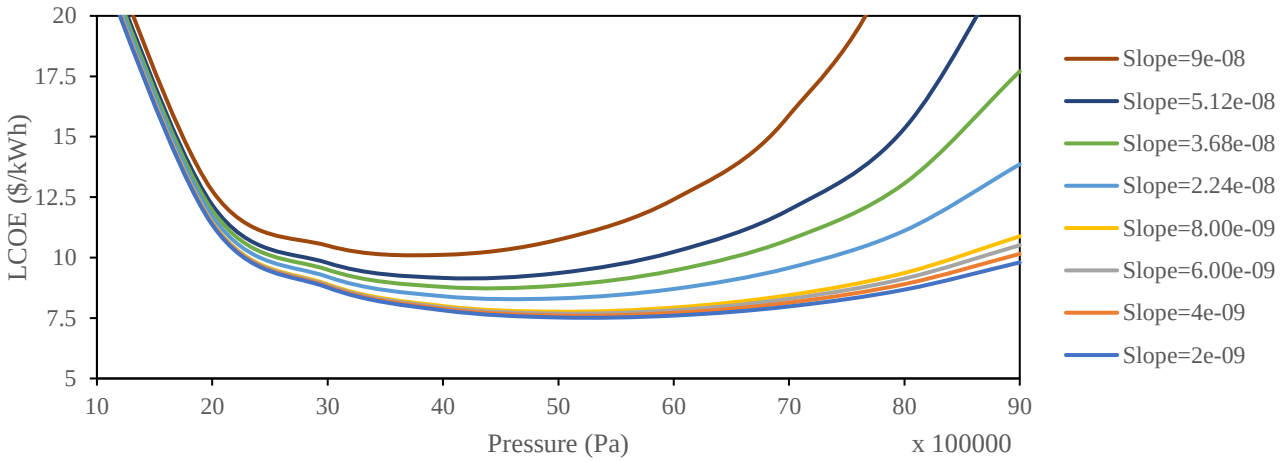

Figure 13: Plot of LCOE against the rate of increase of B vs P

The results obtained ares shown in Figure 13. At 30bar, increasing the rate from $2x10^{-9}$ to $8x10^{-9}$ L/(m^2.h. Pa) (increase done within values of the same order of magnitude) leads to an increase of 1.5% in LCOE. At the same pressure, an increase from $2.24x10^{-8}$ to $5.12x10^{-8}$ L/(m^2.h. Pa) leads to an increase of 6.25% in LCOE. A 4-times increase in value of the rate at a lower order of magnitude yields only a 1.5% increase in LCOE while a 2-times increase in value of the slope at a higher order of magnitude gives an increase in LCOE of 6.25%.

At a higher pressure of 50 bar and using the same range of increase rates of B, the increase in LCOE becomes 3.17% and 18.78% respectively. This is an indication that beyond a certain value of the increase rate, the detrimental effect that rate contributes to LCOE becomes negligible.

4.3.2 EFFECT OF STRUCTURAL PARAMETER ON LCOE

This section is divided into two subsections. Subsection 6.2.1 presents the analysis made when the intercept of the curve of Structural Parameter against Pressure (S vs P) is varied and section 6.2.2 shows results when the slope of the S vs P curve is varied. Table 5 presents the membrane properties and process conditions used in the set-up of the simulation.

Table 5: HTI-CTA membrane properties and Process Conditions

Property	Values	
Area (m^2)	40	
Water Permeability ($L/m^2.h.bar$)	0.42	
Salt permeability ($L/m^2.h$)	0.284	
Slope of B vs P line ($L/(m2.h.\ Pa)$)	$8.357x10^{-8}$	
	LCOE vs Intercept of S vs P curve	LCOE vs Slope of S vs P curve
Structural parameter (m)	$\{1.00x10^{-3} – 1.00x10^{-4}\}$	$1.00x10^{-3}$
Slope of S vs P line (m/Pa)	$2.367x10^{-10}$	$\{2x10^{-10} – 1x10^{-11}\}$
Diffusion coefficient (m^2/s)	$1.48x10^{-9}$	
Mass transfer coefficient ($L/m^2.h$)	300.0	
Hydraulic pressure (bar)	{10 -90}	
Draw flowrate (m^3/s)	$3.5x10^{-4}$	
Feed flowrate (m^3/s)	$3.5x10^{-4}$	
Temperature	298.15	298.15
Na^+ ion (g/L)	68.97	0
Cl^- ion (g/L)	106.51	0

4.3.2.1 Effect of Structural Parameter (Intercept) on LCOE

The graphical representation of the analysis is shown in Figure 14. The intercept is varied from $1x10^{-4} – 1x10^{-3}$ m with the of increase of "S" kept constant.

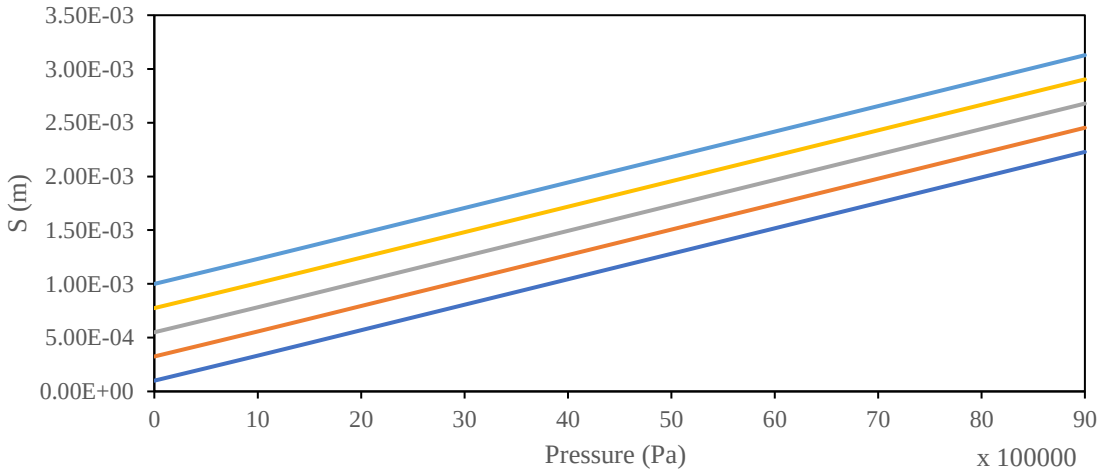

Figure 14: Graphical representation of the variation of intercept with pressure used in the problem set up.

The results obtained are shown in Figure 15 and indicate that at any specific value of pressure, the LCOE increases as the value of intercept increases. Higher values of LCOE indicate less efficiency in power generation (as the cost remains unchanged). For a specific value of intercept, the LCOE reaches a minimum and then increases beyond a certain pressure. This trend is generally observed for Pressure-LCOE relationships as increased pumping costs and decreased power production beyond optimum pressure results in the trend seen.

Increasing the simulation limits show that decreasing the value of intercept from $5.5x10^{-6}$ to $5.5x10^{-7}$m only leads to a 0.22% decrease in LCOE.

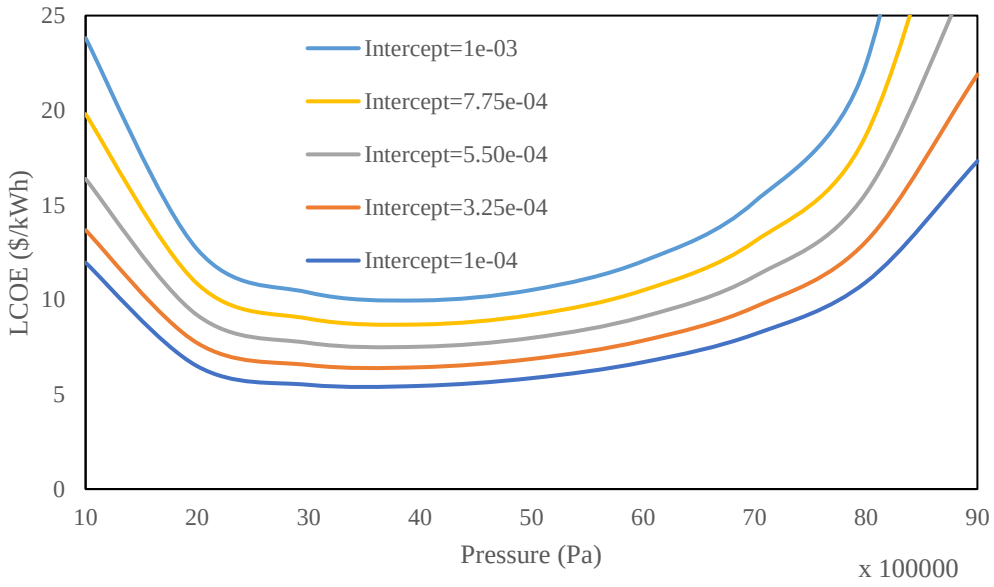

Figure 15: LCOE vs structural parameter

4.3.2.2 Effect of the Rate of Structural Parameter Increase against Pressure on LCOE

Figure 16 shows the graphical setup when the "S" increase rate is varied from $2x10^{-11}$ to $2x10^{-10}$ m/Pa.

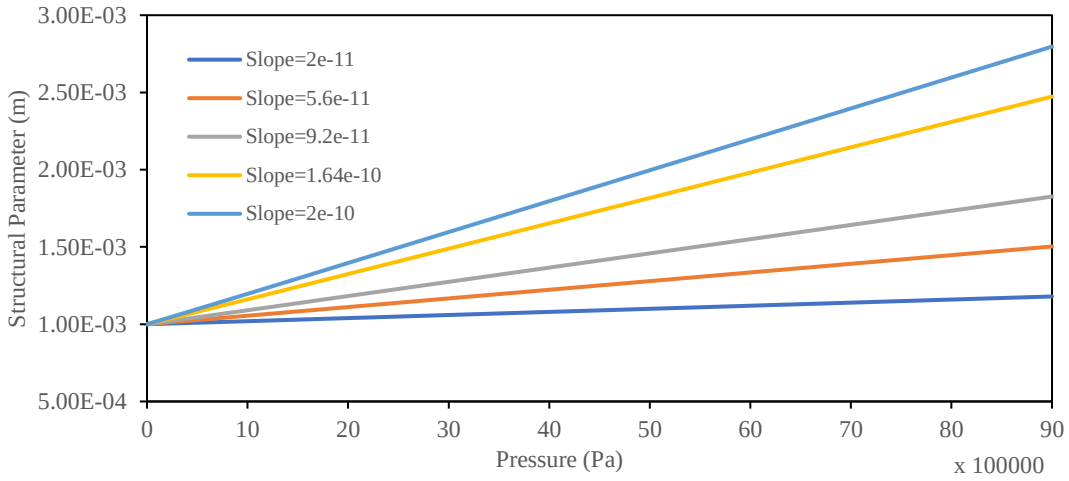

Figure 16:Graphical representation of "S" increase rate

From Figure 17, the results show that increasing the "S" increase rate from $2x10^{-11}$m/Pa to $2x10^{-10}$m/Pa, the LCOE increased by 29.4% at 20bar and 84.5% at 50bar. At lower pressures, the effect of slope on the LCOE is minimal.

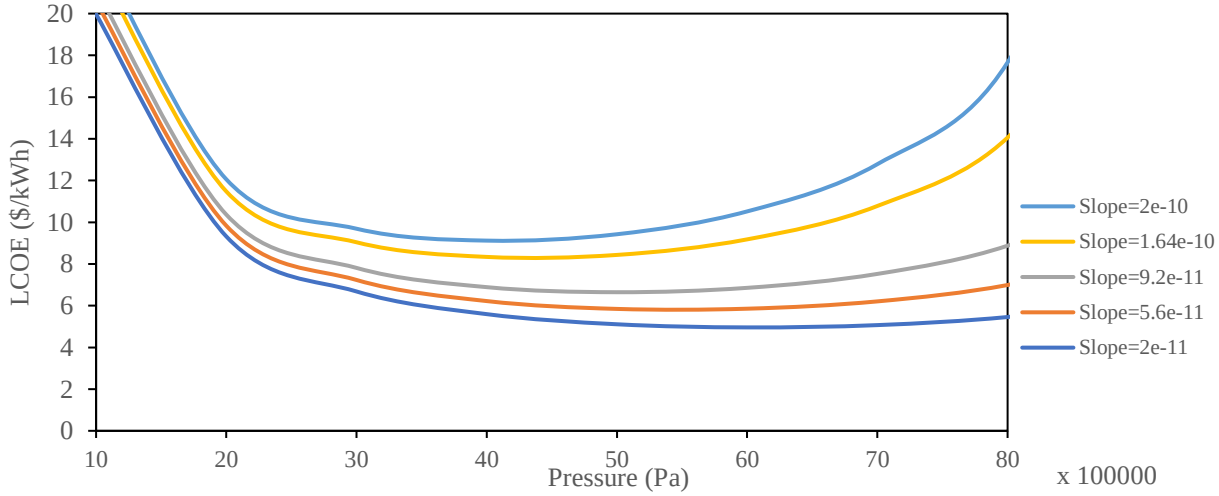

Figure 17: Plot of LCOE vs Pressure at different values of "S" increase rate

For the range studied, the impact of "S" increase rate versus pressure remains appreciable. For example, at 40bar, increasing the rate by a small value from $2x10^{-11}$m/Pa to $5.6x10^{-11}$m/Pa, the LCOE increases by 11.2%.

4.3.3 EFFECT OF WATER PERMEABILITY ON LCOE AND NET POWER

This section presents the effect of water permeability "A" on LCOE. The water permeability was reported to be independent of pressure [58]. Hence, unlike the previous two sections, only the absolute value of salt permeability is varied. Table 6 presents the parameters and process conditions used in the problem setup.

Table 6: HTI-CTA membrane properties and Process Conditions

	Values	
Area (m^2)	40	
Water Permeability (L/m^2.h.bar)	{0.2 – 10}	
Salt permeability (L/m^2.h)	0.284	
Slope of B vs P line (L/(m2.h. Pa))	$8.357x10^{-8}$	
Structural parameter (m)	$1.00x10^{-3}$	
Slope of S vs P line (m/Pa)	$2.369x10^{-10}$	
Diffusion coefficient (m^2/s)	$1.48x10^{-9}$	
Mass transfer coefficient (L/m^2.h)	300.0	
Hydraulic pressure (bar)	{10 -90}	
Draw flowrate (m^3/s)	$3.5x10^{-4}$	
Feed flowrate (m^3/s)	$3.5x10^{-4}$	
Temperature	298.15	298.15
Na^+ ion (g/L)	68.97	0
Cl^- ion (g/L)	106.51	0

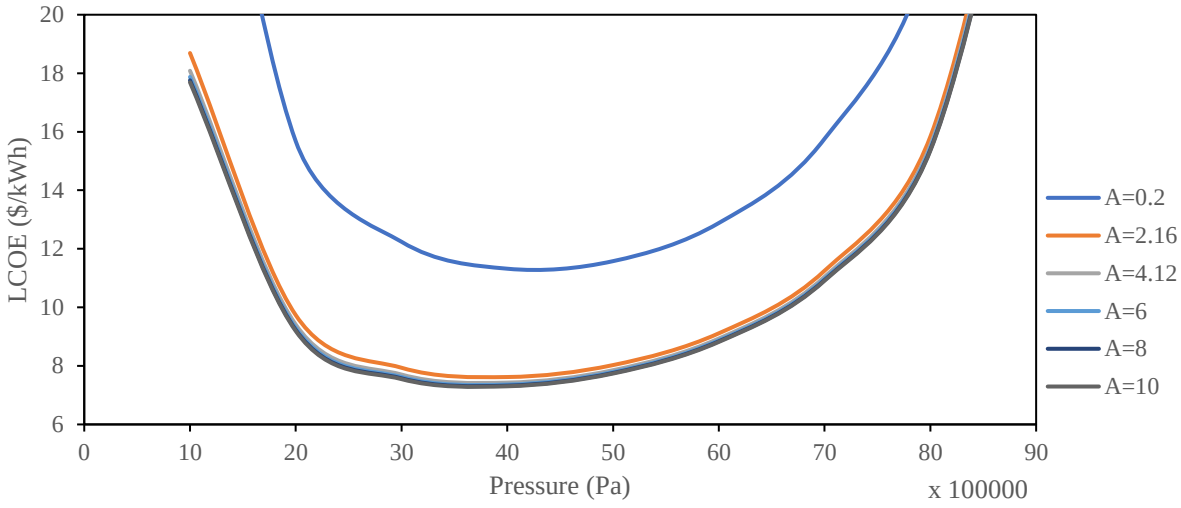

Figure 18: Plot of LCOE vs Pressure at different values of Water Permeability "A" (L/m^2.h.bar)

The results presented in Figure 18 show a negligible decrease in LCOE beyond certain values of water permeability. For clearer data presentation, the LCOE is plotted against water permeability at different values of applied pressure, as shown in Figure 19. The results shown in Figure 19 indicate that although a high value of water permeability is desirable, beyond a certain point, further increase has little impact on LCOE. For example, at 30bar, increasing the "A" from 0.2 to 0.6 L/(m^2.h.bar) decreases the LCOE by 25.35%. Increasing from 2 to 5 L/(m^2.h.bar) causes a decline of 4.28% in LCOE but increasing from 5 to 10 L/(m^2.h.bar) only achieves a 1.42% decline in LCOE.

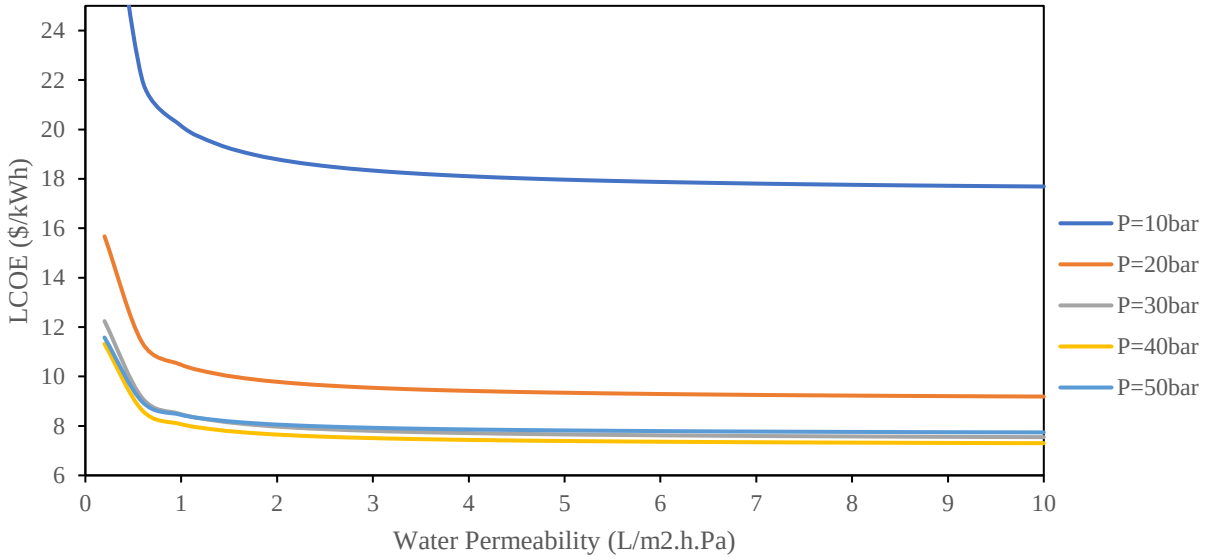

Figure 19: Plot of LCOE against Water Permeability

4.4 OPTIMIZATION STUDIES

This section presents optimization studies that were performed to better understand plant conditions and dimensions that minimize LCOE as well as compare the LCOE values obtained from PRO with other renewable energy technologies.

Section 4.4.1 shows the LCOE obtainable from using an ideal membrane and at 100% efficiency of mechanical components.

Section 4.4.2 presents information on the LCOE obtained using current state of the art PRO membrane operating with perfect efficiency of mechanical components.

Section 4.5 shows the results for a PRO plant taking into account efficiencies of the mechanical components and the results obtained from the three sections are compared with the LCOE of other renewable energy systems using global average values from the IRENA database [56].

4.4.1 LCOE CALCULATIONS WITH IDEAL MEMBRANE AND 100% EFFICIENCY OF MECHANICAL COMPONENTS

An optimization was carried out using the DAKOTA optimization tool with the LCOE as the objective function to be minimized. The flowrates of the draw and feed, applied pressure and

membrane area were the parameters. Table 7 shows the membrane properties used to represent ideal conditions, as well as process and stream conditions used in the problem set up.

Table 7: Ideal Membrane Properties and Stream Conditions

Property	Values	
Area (m^2)	{45,000 -200,000}	
Water Permeability ($L/m^2.h.bar$)	6	
Salt permeability ($L/m^2.h$)	0	
Structural parameter (m)	0	
Diffusion coefficient (m^2/s)	$1.48x10^{-9}$	
Mass transfer coefficient ($L/m^2.h$)	99.0	
Hydraulic pressure (bar)	{40 – 90}	
Draw flowrate (m^3/s)	{0.15 – 0.5}	
Feed flowrate (m^3/s)	{0.3 – 0.7}	
Temperature	298.15	298.15
Na^+ ion (g/L)	68.97	13.8
Cl^- ion (g/L)	106.51	21.3

Table 8: Optimization Results for Ideal Membrane

Pressure (bar)	42.69
Draw flowrate (m^3/s)	0.2855
Feed flowrate (m^3/s)	0.477
Area (m^2)	71,215
LCOE ($/kWh)	0.0704

The results obtained from the optimization study is shown in Table 8. This value represents the lowest achievable LCOE for a single stage system using the specified process conditions and stream salinities. Levelized cost of $0.0704/kWh was achieved which is better than Geothermal energy, offshore wind and CSP using 2019 global average value reported by IRENA [56].

4.4.2 LCOE CALCULATIONS WITH REAL MEMBRANE PERFORMANCE AND 100% EFFICIENCY OF MECHANICAL COMPONENTS

Using the mass transport parameters of a real membrane, this section reports the LCOE for a full-scale plant with 100% efficiency of mechanical components. The process conditions and membrane properties used in this set up are given in Table 9.

Table 9:Properties of Struab et al. HTI-CTA Membrane and Stream Properties

Property	Values	
Area (m^2)	{1,000 – 500,000}	
Water Permeability ($L/m^2.h.bar$)	2.49	
Salt permeability ($L/m^2.h$)	0.39	
Structural parameter (m)	$5.64x10^{-4}$	
Diffusion coefficient (m^2/s)	$1.48x10^{-9}$	
Mass transfer coefficient ($L/m^2.h$)	99.0	
Hydraulic pressure (bar)	{30 -90}	
Draw flowrate (m^3/s)	{2.65e-03 -13.25}	
Feed flowrate (m^3/s)	{2.65e-03 -13.25}	
Temperature	298.15	298.15
Na^+ ion (g/L)	68.97	13.8
Cl^- ion (g/L)	106.51	21.3

Table 10: Optimization Results using Real Membrane

Pressure (bar)	48.48
Draw flowrate (m^3/s)	0.2853
Feed flowrate (m^3/s)	0.4437
Area (m^2)	137,255
LCOE ($/kWh)	0.1255

The results for the optimization study is presented in Table 10. Nonidealities in the membrane leads to 92.7% increase in the required membrane area as well as 78.5% increase in the value of LCOE. At this value of LCOE, PRO technology is only better than CSP [56].

4.5 COMPARING PRO WITH OTHER RENEWABLE ENERGY SOURCES

The International Renewable Energy Agency (IRENA) released the Renewable Energy power generation costs for year 2019 [56]. The reported results in Figure 20 are used as a basis of comparing between different renewable energy sources. The values reported are global averages.

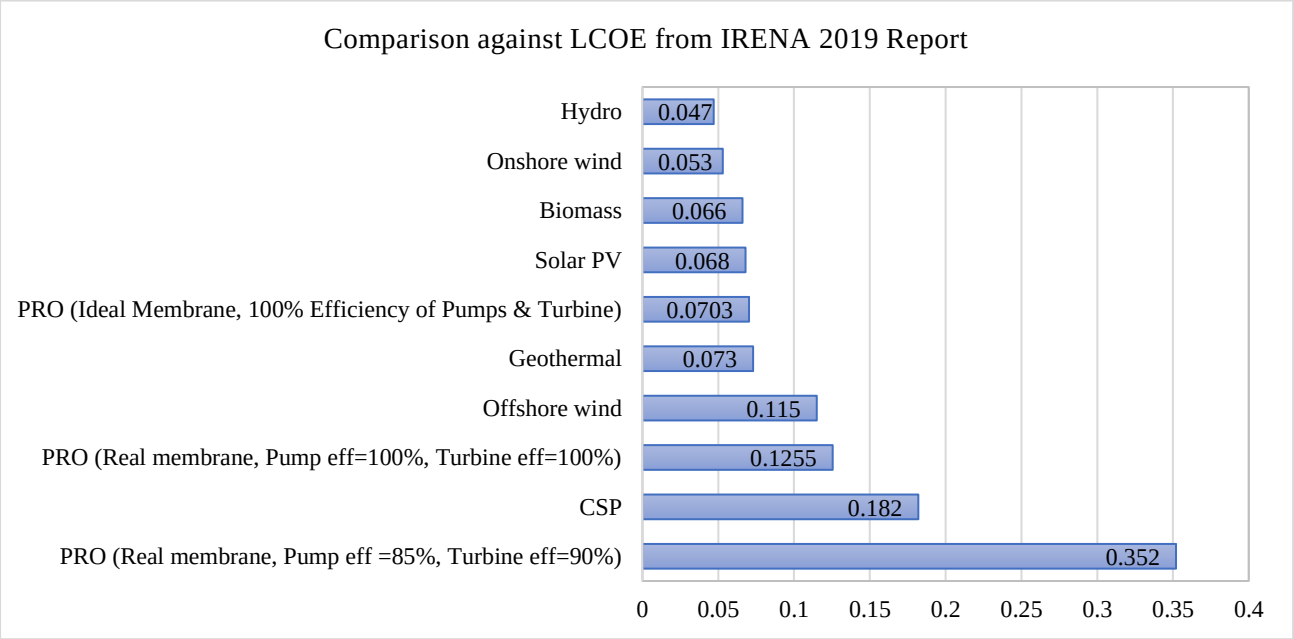

Figure 20: 2019 IRENA Reported LCOE values compared with PRO

Figure 20 shows that the LCOE of PRO with real membrane performance and considering equipment efficiencies is higher than other sources. However, it is comparable to both Solar Photovoltaics and Concentrated Solar Power considering their costs at the start of their production in 2010 as shown in Figure 21.

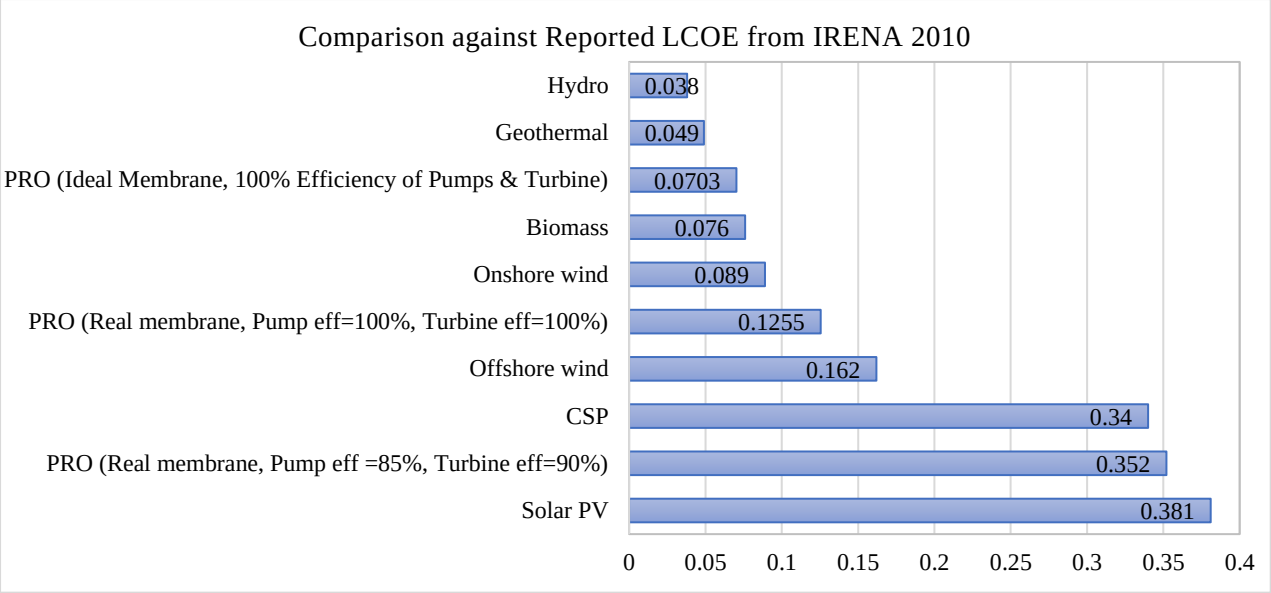

Figure 21: 2010 IRENA Reported LCOE values compared with PRO

4.6 MULTI-STAGE ANALYSIS

PRO and RO systems have many similarities and it has been shown that multistage operation improves the energetic performance of a reverse osmosis process [59],[60], [61]. Wei et al. [59] show that for a reverse osmosis process, the energetic benefits gotten from staged designs is confounded by increased costs of membrane area – although with careful design, the energetic benefits could outweigh costs.

Some interesting multistage design for PRO has been reported in literature. Chung et al. [62] classified all two-module multistage designs into two broad families – interstage pressure control and input exergy control. Interstage Pressure control refers to designs with either a pump (for interstage pressurization) or a turbine (for interstage depressurization) between membrane modules. Pressure control is important in reducing entropy generation because it helps to achieve a more uniform osmotic driving force [63], [64].

Input exergy control refers to a design philosophy that allows for modification to the draw and feed streams as they enter the process. This control method seeks to maintain the salinity gradient across the membrane in both stages.

Altaee et al. [65] and Li [66] studied dual stage systems that can be classified as Interstage pressure control. While Altaee et al. had design with interstage pressurization, Li had interstage depressurization.

He et al. [67] introduced four designs for two-stage PRO systems and each design is named depending on if the draw or feed solution is split on entering the process. Their design can be classified as Input Exergy Control. Of the four designs, two of them are studied in this work.

Designs Evaluated

A single stage system with the process conditions shown in Table 11 is set as a benchmark against which different multistage designs are evaluated.

Table 11: Input Properties Used in Evaluating the Benchmark Single Stage System

Property	Values	
Area (m^2)	137255	
Water Permeability ($L/m^2.h.bar$)	2.49	
Salt permeability ($L/m^2.h$)	0.39	
Structural parameter (m)	$5.64x10^{-4}$	
Diffusion coefficient (m^2/s)	$1.48x10^{-9}$	
Mass transfer coefficient ($L/m^2.h$)	99.0	
Hydraulic pressure (bar)	48.48	
Draw flowrate (m^3/s)	0.2853	
Feed flowrate (m^3/s)	0.6758	
Temperature	298.15	298.15
Na^+ ion (g/L)	68.97	0
Cl^- ion (g/L)	106.51	0

The resultant net power produced and LCOE is 2,233.88kW and $0.0693/kWh respectively. The designs evaluated are Differentiated Draw Continuous Feed (DDCF) and Continuous Draw Differentiated Feed (CDDF).

4.6.1 DIFFERENTIATED DRAW CONTINUOUS FEED (DDCF)

The configuration shown in Figure 22 represents the DDCF design and is evaluated on the basis of net power produced as well as the resultant LCOE. Pressurized undiluted draw enters into both stages (stage 1 and stage 2) while the feed moves from stage 2 to stage 1 in counter flow direction.

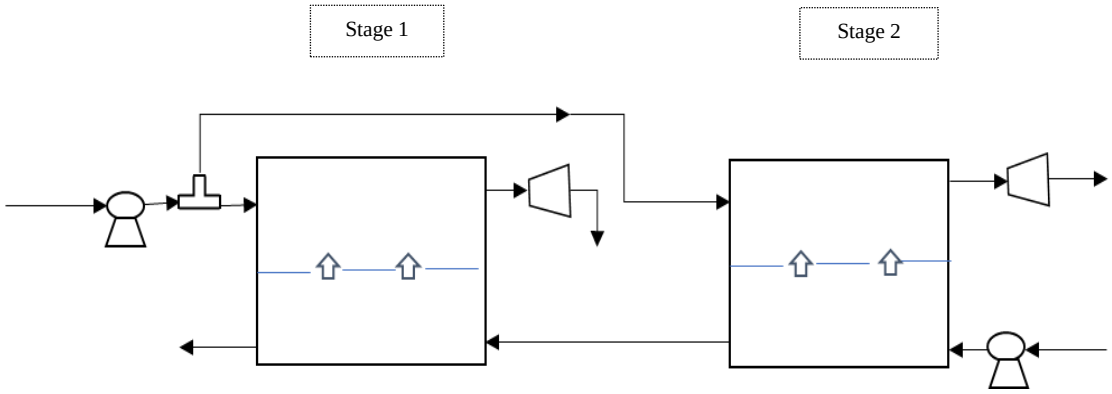

Figure 22: Differentiated Draw Continuous Feed Configuration. Figure Adapted from [67]

One clear advantage of this design is that salinity gradient across membrane 2 is higher than would otherwise have been had the draw moved continuously from stage 1 to 2.

The process conditions and membrane properties used are shown in Table 12. The split ratio indicates the ratio of total membrane area as well as the ratio of the total draw flow rate allocated to each stage. This ratio adds up to 1.

Table 12: Input Properties Used in Evaluating DDCF Configuration

Property	Values	
Total Membrane area (m^2)	137,255	
Total Draw Flowrate (m^3/s)	0.2852	
Total Feed flowrate (m^3/s)	0.6758	
Property	Values	
	Stage 1	Stage 2
Split Ratio	{0.01 – 0.90}	{0.99 – 0.10}
Area (m^2)	{1,372.55 – 123,529.50}	{135,882.45 – 13,725.50}
Draw flowrate (m^3/s)	{0.0028523 - 0.25670}	{0.2824 – 0.02852}
Property	Values	

Table 12: Input Properties Used in Evaluating DDCF Configuration (continued)

Property	Values	
Water Permeability (L/m^2.h.bar)	2.49	
Salt permeability (L/m^2.h)	0.39	
Structural parameter (m)	5.64x10^{-4}	
Diffusion coefficient (m^2/s)	1.48x10^{-9}	
Mass transfer coefficient (L/m^2.h)	99.0	
Hydraulic pressure (bar)	48.48	
Temperature	298.15	298.15
Na^+ ion (g/L)	68.97	0
Cl^- ion (g/L)	106.51	0

The power produced by both turbines (Turbine 1 and Turbine 2) are shown against split ratio of membrane 1 in Figure 23. At equal split of the membranes (split ratio of 50:50), Turbine 2 (associaed with membrane 2) produces 4.85% more power than Turbine 1 because of higher salinity graient across Membrane 2.

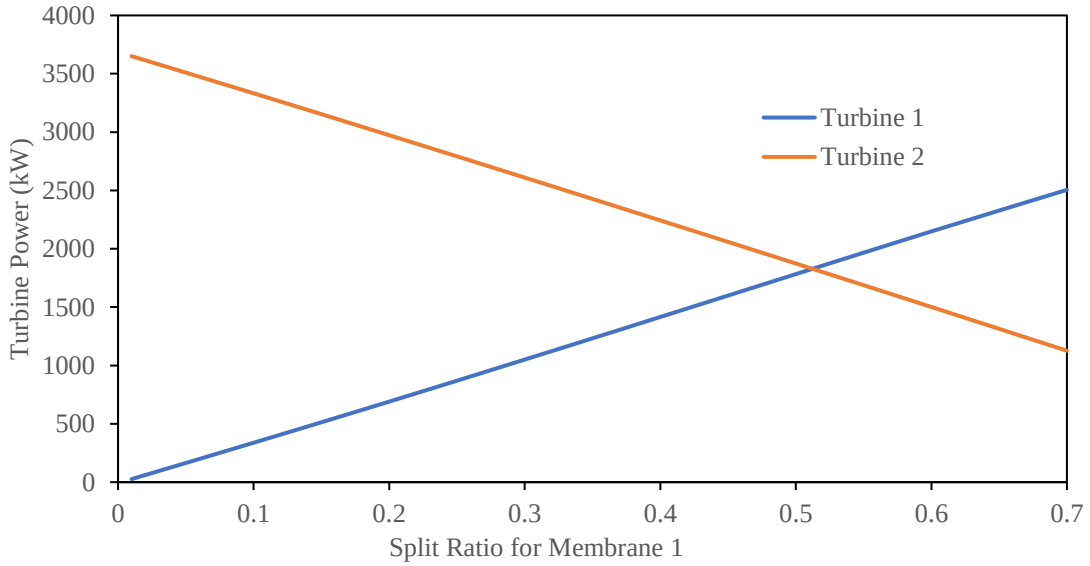

Figure 23: Power of Turbines against Split ratio of Membrane 1

The split ratio affects the net power produced by the system. A split ratio of 0.3 (Membrane 1 gets 30% while Membrane 2 gets 70% of both total area and draw) does not give the same net power as a split ratio of 0.7. From Figure 24, the Net Power produced is higher at a ratio of 0.3 than 0.7 and the difference is 29.19kW.

.

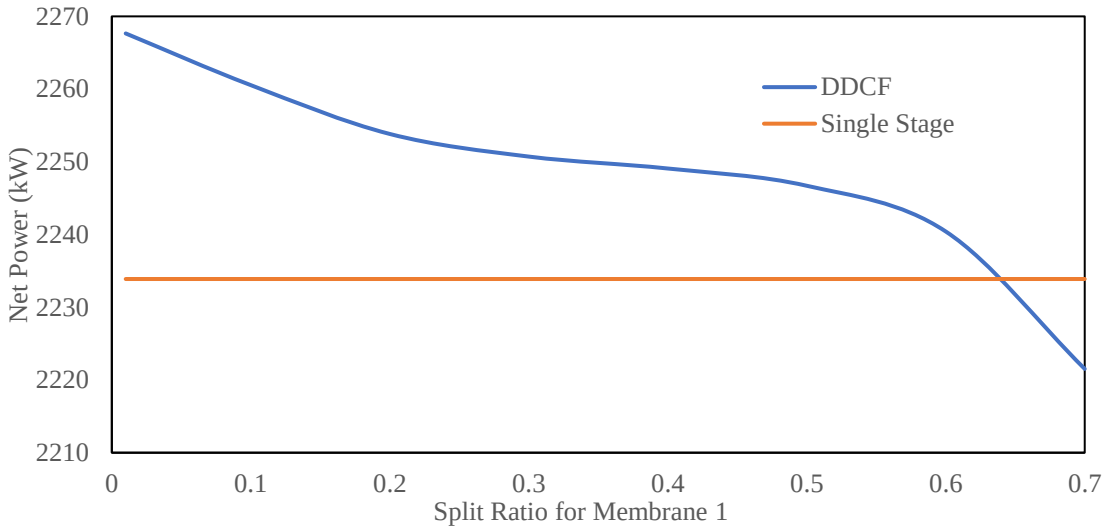

Figure 24: Net Power (kW) produced against Split ratio for Membrane 1

There are two effects contributing to power production. The first is that to reduce irreversible losses, a larger membrane area is required and the second is the salinity gradient across the membrane – higher gradient increases the driving force across the membrane. Stage 1 always has lower gradient across it because the feed stream that enters in is concentrated via reverse salt flux on leaving Stage 2. Although assigning a larger portion of the total area to Stage 1 (ratio > 0.5) gives larger turbine power to Turbine 1 compared to Turbine 2, the net power produced is lower overall. This could be an indication that salinity gradient plays a larger role in power generation than membrane area.

Comparing the net power produced from the DDCF design against that of Single stage, lower split ratio for Membrane 1 is more favorable to power production. At ratio > 0.65, the multistage design produces lower power than for a single stage system.

On the basis of LCOE, as seen from Figure 25, as expected, the trend is the mirror image of the Net Power. Compared to single stage LCOE value, only split ratio below 0.08 gives LCOE

values lower than single stage. However, the LCOE is just 0.25% better than the value of single stage.

It would seem that the extra power generated in the DDCF design is not enough to justify the cost of production.

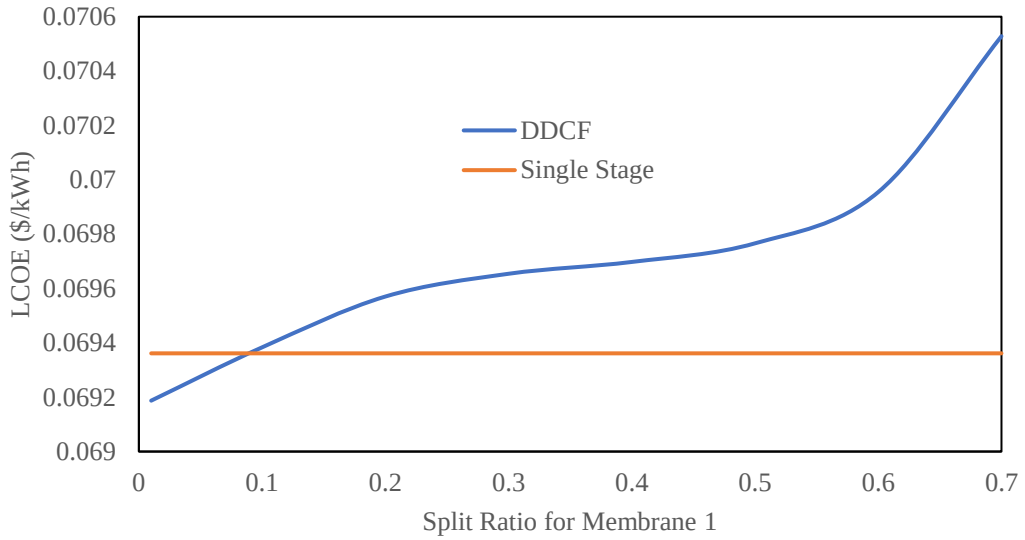

Figure 25: LCOE against Membrane 1 Split Ratio

4.6.2 CONTINUOUS DRAW DIFFERENTIATED FEED (CDDF)

The configuration shown in Figure 26 represents the CDDF design and is evaluated on the basis of net power produced and LCOE. In this configuration, undiluted feed enters both stages while the draw moves from stage 1 into stage 2.

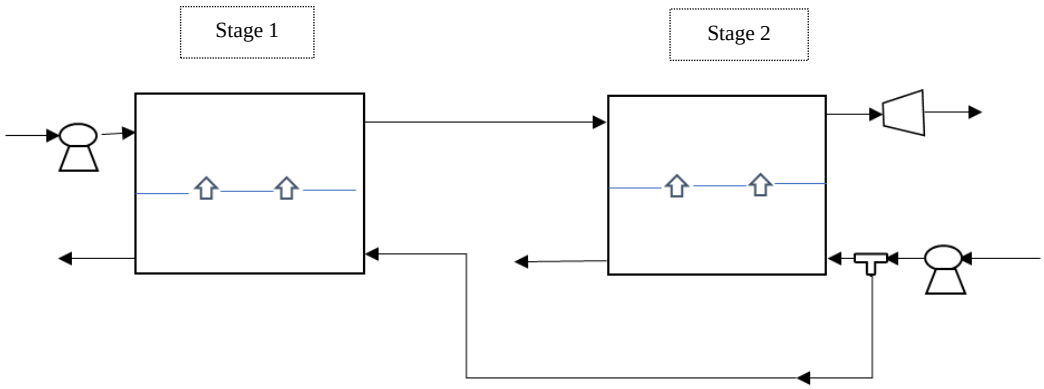

Figure 26: Continuous Draw Differentiated Feed Configuration. Figure Adapted from [35]

The process conditions and membrane properties used are shown in Table 13. The split ratio indicates the ratio of total membrane area as well as the ratio of the total draw flow rate allocated to each stage. This ratio adds up to 1.

Table 13: Input Properties Used in Evaluating CDDF Configuration

Property	Values	
Total Membrane area (m^2)	137,255	
Total Draw Flowrate (m^3/s)	0.2852	
Total Feed flowrate (m^3/s)	0.6758	
	Stage 1	Stage 2
Split Ratio	{0.90 – 0.15}	{0.1 – 0.85}
Area (m^2)	{123,529.50 – 20,588.25}	{13,725.50 – 116,666.75}
Feed flowrate (m^3/s)	{0.60822 – 0.10137}	{0.06758 – 0.57443}
Water Permeability ($L/m^2.h.bar$)	2.49	
Salt permeability ($L/m^2.h$)	0.39	
Structural parameter (m)	$5.64x10^{-4}$	
Diffusion coefficient (m^2/s)	$1.48x10^{-9}$	
Mass transfer coefficient ($L/m^2.h$)	99.0	
Hydraulic pressure (bar)	48.48	
Temperature	298.15	298.15
Na^+ ion (g/L)	68.97	0
Cl^- ion (g/L)	106.51	0

The split ratio has an effect on the net power produced. From Figure 27, assigning 80% of the total area and total feed to Stage 1 produces 70.7kW less power than assigning 80% of total area and feed to Stage 2. This design favors allocation of the larger percentage of area and feed to the second stage. This is because lower volumetric flow of the feed in Stage 1 leads to lower draw dilution before entering Stage 2. However, this design produces less power than a single stage system.

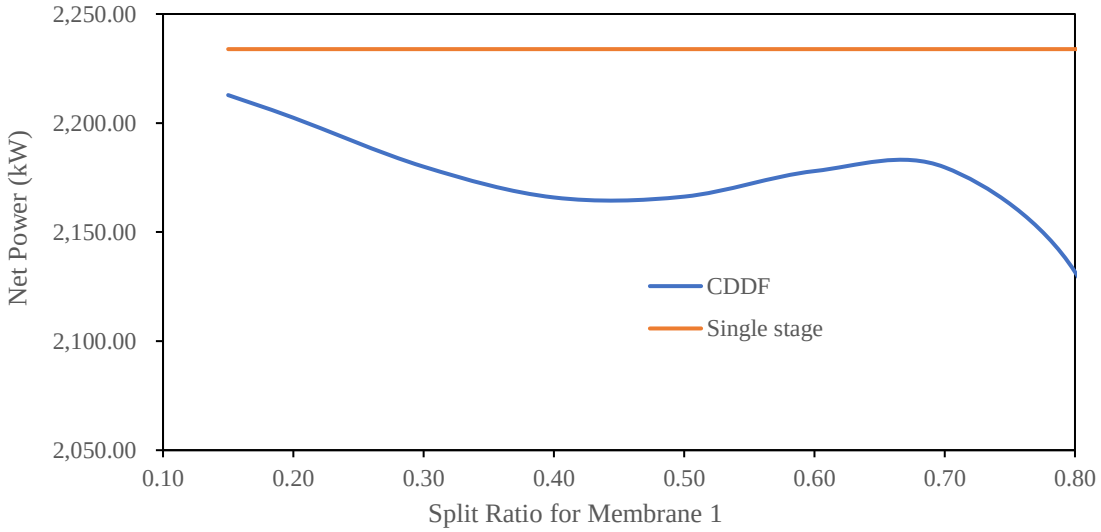

Figure 27: Net Power (kW) produced against Split ratio for Membrane 1

The LCOE for the CDDF configuration is higher than that of single stage for all values of split ratio as shown in Figure 28.

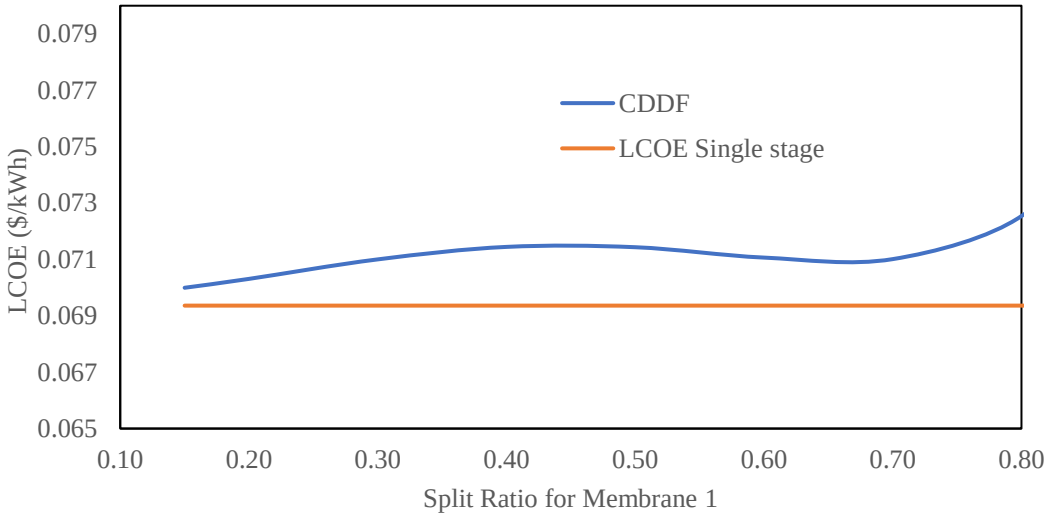

Figure 28: LCOE ($/kWh) against Membrane 1 Split Ratio

4.6.3 DIFFERENTIATED DRAW CONTINUOUS FEED (DDCF) USING PRODUCED WATER AND SEAWATER

The result from the single stage optimization gave the dimensions of the plant as well as stream volumes that minimized LCOE as shown in Table 14. The net power produced is also shown.

Only DDCF is evaluated because it has been shown that even with fresh water, the CDDF did not give more power than the single stage.

Table 14: Single Stage Optimized Result

Pressure (bar)	48.48
Draw flowrate (m^3/s)	0.2853
Feed flowrate (m^3/s)	0.4437
Area (m^2)	137,255
Net Power (kW)	849.14
LCOE ($/kWh)	0.1255

Table 15 presents the information used to set up the analysis using the Differentiated Draw Continuous Feed (DDCF) configuration.

Table 15: Input Properties Used in Evaluating DDCF Configuration

Property	Values	
Total Membrane area (m^2)	137,255	
Total Draw Flowrate (m^3/s)	0.2852	
Total Feed flowrate (m^3/s)	0.4437	
	Stage 1	Stage 2
Split Ratio	{0.01 – 0.90}	{0.99 – 0.10}
Area (m^2)	{1,372.55 – 123,529.50}	{135,882.45 – 13,725.50}
Draw flowrate (m^3/s)	{0.00285 - 0.2567}	{0.2824 – 0.02852}
Water Permeability ($L/m^2.h.bar$)	2.49	
Salt permeability ($L/m^2.h$)	0.39	
Structural parameter (m)	$5.64x10^{-4}$	
Diffusion coefficient (m^2/s)	$1.48x10^{-9}$	
Mass transfer coefficient ($L/m^2.h$)	99.0	
Hydraulic pressure (bar)	48.48	
Temperature	298.15	298.15
Na^+ ion (g/L)	68.97	13.8
Cl^- ion (g/L)	106.51	21.3

The results of net power against split ratio in Figure 29 show that at ratio < 0.15, the net power produced is less than that of single stage.

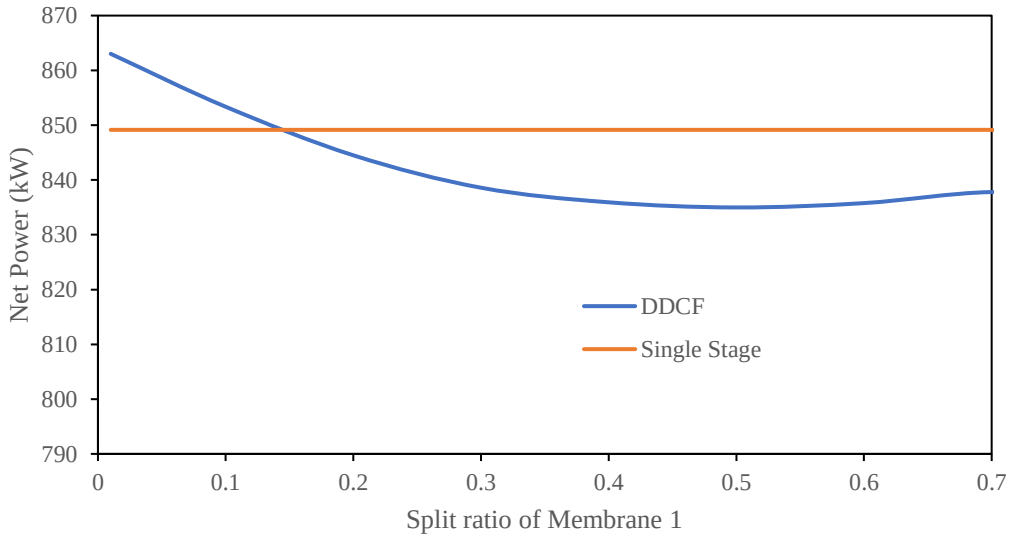

Figure 29: Net Power (kW) produced against Split ratio for Membrane 1

The plot of LCOE Figure 30 show that the LCOE of the single stage is lower than the LCOE of DDCF at all values of split ratio.

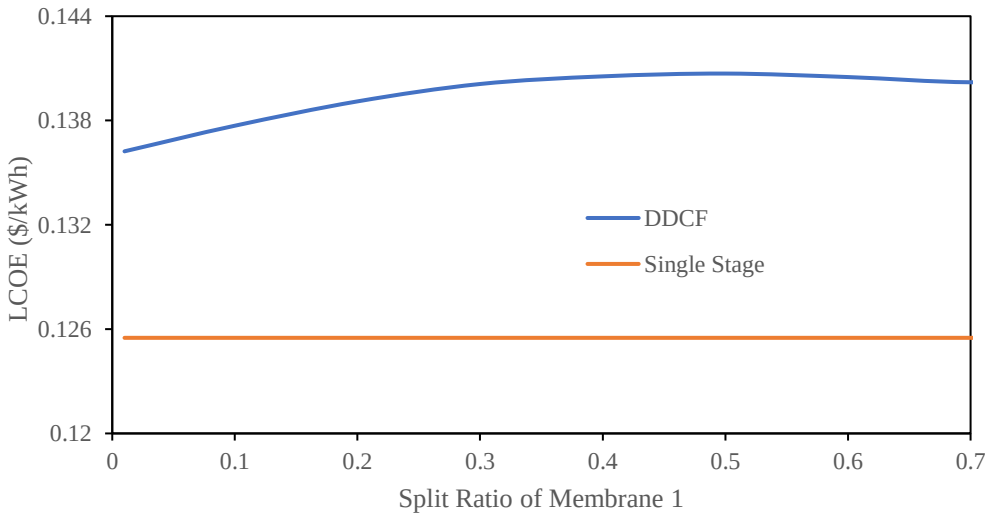

Figure 30: LCOE ($/kWh) against Membrane 1 Split Ratio

5 CONCLUSION AND FUTURE WORK

In this work, techno-economic analysis was carried out on full scale single stage and multistage pressure retarded osmosis systems to determine its economic viability. The draw and feed solutions were Produced water (3M NaCl) and Seawater (0.6M NaCl) respectively. The techno-economic parameter of interest is the Levelized cost of electricity (LCOE) which depends on the cost of energy produced as well as the total amount of electrical energy produced.

Each module making up the PRO system was costed based on a relevant attribute (e.g., turbines costed on the basis of power produced). The Chemical Engineering Plant Cost Index (CEPCI) was used to account for inflation – thus bringing the capital costs to the year of interest/project execution.

Although much focus in literature has been on the energetic performance of PRO systems, this work shows that energetic and economic optimum occur at different system conditions. Hence conditions that maximize energy production might be economically unfeasible. An example can be seen in the fact that while larger membrane areas minimize irreversible losses, they incur a penalty by increasing capital expenditure. Similarly, larger pumping power also incurs higher costs. System size might be advantageous in terms of the benefits to economies of scale; however, scale limits the operating conditions that minimizes LCOE. This means that larger plants would be more difficult to operate as the operating constraints are narrower.

Membrane properties play an important role in the techno-economics of PRO systems. For the same membrane area (and costs), a membrane with higher water permeability and lower salt permeability and structural parameter produces more energy. Hence, more energy is produced at the same cost lowering LCOE. A set of analyses was performed using a membrane with pressure dependent salt permeability and structural parameter with Produced water and Fresh

Water as draw and feed respectively. The results show that beyond a water permeability value of 5L/(m^2.h.bar), increasing the water permeability to a value of 10 L/(m^2.h.bar), gives a mere 1.42% decrease in LCOE suggesting little incremental advantage by increasing water permeability beyond a certain point. On the other hand, minimum LCOE was achieved at a salt permeability of 0 L/(m^2.h). For structural parameter, moving from a value of $5.5x10^{-6}$m, to $5.5x10^{-7}$m, the decrease in LCOE is a meagre 0.22%. This is an important future work – improving the membrane properties to these benchmark points.

Optimization studies were carried out to determine the system size, operating pressure and stream flowrates to minimize the objective function LCOE. Both ideal and real membranes were used. Using Ideal membrane and keeping the efficiency of all mechanical components at 100%, the LCOE achieved is $0.074/kWh which is comparable to Geothermal energy and better than Offshore wind and CSP using the International Renewable Energy Agency (IRENA) 2019 global average values for LCOE. With real membranes, the LCOE increases to $0.1255/kWh which is better than only CSP. Using real membranes and considering efficiencies of mechanical components, the LCOE increases to $0.352/kWh – higher than all other renewable energy sources.

Multistage analysis was carried out using two design configurations – on that supplies fresh draw to each module and the other that supplies fresh feed to each module. Using produced water and fresh water as draw and feed respectively, only the design which supplies fresh draw produced more power than the single stage system. The power produced depends highly on the ratio of membrane area and draw flowrate allocated to each stage. Even with this design supplying fresh feed, wrong allocation of area between stages led to power production lower than single stage. Using Produced water and Seawater, more power was produced than the single stage system at some ratio allocation of area and draw flowrate but the LCOE remained

higher than for single stage at all ratio allocation indicating that extra power produced does not justify the cost of production.

Future work can be two-fold – the first is by continuous improvment of membrane properties to maximize power production at lower cost. The second deals with the cost angle to the LCOE. From solar photovoltaics, IRENA reports that costs have declined by 82% from 2010 to 2019. However, the efficiency of panels has increased by 30% within the same time period. This is an indication that market forces of incentivizing demand for renewable energy technology remains the largest driver of adoption. Increased demand then improves technology demand until competition drives lower prices without incentives.

PRO has another advantage that other renewable energy technologies do not have – the use of hypersaline produced water. As oil and gas reservoirs mature, they produce more water. Depending on the salinity, regulation mandates the drilling of deep disposal wells which increase the cost of the operation. If the capital cost for PRO system is channeled from this mandated disposal system, then where once produced water was a total liability, it becomes a source of generating electricity and carbon credits.

REFERENCES

[1] Martin I. Hoffert *et al.*, "Advanced Technology Paths to Global Climate Stability: Energy for a Greenhouse Planet," *Science (80-.).*, vol. 298, no. 5595, pp. 981–987, 2002.

[2] S. Chu and A. Majumdar, "Opportunities and challenges for a sustainable energy future," *Nature*, vol. 488, no. 7411, pp. 294–303, 2012, doi: 10.1038/nature11475.

[3] H. W. Chung, L. D. Banchik, J. Swaminathan, and J. H. Lienhard V, "On the present and future economic viability of stand-alone pressure-retarded osmosis," *Desalination*, vol. 408, pp. 133–144, 2017, doi: 10.1016/j.desal.2017.01.001.

[4] "What Is Grid Parity and Why Does It Matter? | Climate Reality." https://www.climaterealityproject.org/blog/what-grid-parity-and-why-does-it-matter (accessed May 07, 2021).

[5] R. A. Tufa, E. Curcio, E. Fontananova, and G. Di Profio, *3.8 Membrane-Based Processes for Sustainable Power Generation Using Water: Pressure-Retarded Osmosis (PRO), Reverse Electrodialysis (RED), and Capacitive Mixing (CAPMIX)*, no. December. Elsevier Ltd., 2017.

[6] N. Y. Yip, D. A. Vermaas, K. Nijmeijer, and M. Elimelech, "Thermodynamic, energy efficiency, and power density analysis of reverse electrodialysis power generation with natural salinity gradients," *Environ. Sci. Technol.*, vol. 48, no. 9, pp. 4925–4936, 2014, doi: 10.1021/es5005413.

[7] M. C. Hatzell, R. D. Cusick, and B. E. Logan, "Capacitive mixing power production from salinity gradient energy enhanced through exoelectrogen-generated ionic currents," *Energy Environ. Sci.*, vol. 7, no. 3, pp. 1159–1165, 2014, doi: 10.1039/c3ee43823f.

[8] X. Zhu, W. Yang, M. C. Hatzell, and B. E. Logan, “Energy recovery from solutions with different salinities based on swelling and shrinking of hydrogels,” *Environ. Sci. Technol.*, vol. 48, no. 12, pp. 7157–7163, 2014, doi: 10.1021/es500909q.

[9] A. Achilli and A. E. Childress, “Pressure retarded osmosis: From the vision of Sidney Loeb to the first prototype installation - Review,” *Desalination*, vol. 261, no. 3, pp. 205–211, 2010, doi: 10.1016/j.desal.2010.06.017.

[10] A. Achilli, T. Y. Cath, and A. E. Childress, “Power generation with pressure retarded osmosis: An experimental and theoretical investigation,” *J. Memb. Sci.*, vol. 343, no. 1–2, pp. 42–52, 2009, doi: 10.1016/j.memsci.2009.07.006.

[11] R. Pattle, “NATU RE October 2, 1954,” *Nature*, vol. 174, no. 1953, p. https://doi.org/10.1038/174660a0, 1954.

[12] S. Loeb, “Production of energy from concentrated brines by pressure-retarded osmosis. I. Preliminary technical and economic correlations,” *J. Memb. Sci.*, vol. 1, no. C, pp. 49–63, 1976, doi: 10.1016/s0376-7388(00)82257-7.

[13] S. Loeb, F. Van Hessen, and D. Shahaf, “Production of energy from concentrated brines by pressure-retarded osmosis. II. Experimental results and projected energy costs,” *J. Memb. Sci.*, vol. 1, no. C, pp. 249–269, 1976, doi: 10.1016/s0376-7388(00)82271-1.

[14] S. Loeb, “One hundred and thirty benign and renewable megawatts from Great Salt Lake? The possibilities of hydroelectric power by pressure-retarded osmosis,” *Desalination*, vol. 141, no. 1, pp. 85–91, 2001, doi: 10.1016/S0011-9164(01)00392-7.

[15] American Water Works Association, *M61 Desalination of Seawater*. 2011.

[16] K. L. Lee, R. W. Baker, and H. K. Lonsdale, “Membranes for power generation by pressure-retarded osmosis,” *J. Memb. Sci.*, vol. 8, no. 2, pp. 141–171, 1981, doi:

10.1016/S0376-7388(00)82088-8.

[17] S. Loeb, “Energy production at the Dead Sea by pressure-retarded osmosis: Challenge or chimera?,” *Desalination*, vol. 120, no. 3, pp. 247–262, 1998, doi: 10.1016/S0011-9164(98)00222-7.

[18] N. Y. Yip *et al.*, “Thin-film composite pressure retarded osmosis membranes for sustainable power generation from salinity gradients,” *Environ. Sci. Technol.*, vol. 45, no. 10, pp. 4360–4369, 2011, doi: 10.1021/es104325z.

[19] S. E. Skilhagen, J. E. Dugstad, and R. J. Aaberg, “Osmotic power - power production based on the osmotic pressure difference between waters with varying salt gradients,” *Desalination*, vol. 220, no. 1–3, pp. 476–482, 2008, doi: 10.1016/j.desal.2007.02.045.

[20] K. Gerstandt, K. V. Peinemann, S. E. Skilhagen, T. Thorsen, and T. Holt, “Membrane processes in energy supply for an osmotic power plant,” *Desalination*, vol. 224, no. 1–3, pp. 64–70, 2008, doi: 10.1016/j.desal.2007.02.080.

[21] F. Helfer, C. Lemckert, and Y. G. Anissimov, “Osmotic power with Pressure Retarded Osmosis: Theory, performance and trends - A review,” *J. Memb. Sci.*, vol. 453, pp. 337–358, 2014, doi: 10.1016/j.memsci.2013.10.053.

[22] B. J. Feinberg, G. Z. Ramon, and E. M. V. Hoek, “Scale-up characteristics of membrane-based salinity-gradient power production,” *J. Memb. Sci.*, vol. 476, pp. 311–320, 2015, doi: 10.1016/j.memsci.2014.10.023.

[23] Q. A. Khasawneh, B. Tashtoush, A. Nawafleh, and B. Kan’an, “Techno-economic feasibility study of a hypersaline pressure-retarded osmosis power plants: Dead sea–red sea conveyor,” *Energies*, vol. 11, no. 11, pp. 1–18, 2018, doi: 10.3390/en11113118.

[24] A. Ansari and M. Abbaspour, “Modelling and economic evaluation of pressure-retarded

osmosis power plant case study: Iran," *Int. J. Ambient Energy*, vol. 40, no. 1, pp. 69–81, 2019, doi: 10.1080/01430750.2017.1354323.

[25] A. Zuber, R. F. Checoni, and M. Castier, "Thermodynamic properties of aqueous solutions of single and multiple salts using the Q-electrolattice equation of state," *Fluid Phase Equilib.*, vol. 362, pp. 268–280, 2014, doi: 10.1016/j.fluid.2013.10.021.

[26] M. F. Naguib, J. Maisonneuve, C. B. Laflamme, and P. Pillay, "Modeling pressure-retarded osmotic power in commercial length membranes," *Renew. Energy*, vol. 76, no. November 2009, pp. 619–627, 2015, doi: 10.1016/j.renene.2014.11.048.

[27] A. P. Straub, S. Lin, and M. Elimelech, "Module-scale analysis of pressure retarded osmosis: Performance limitations and implications for full-scale operation," *Environ. Sci. Technol.*, vol. 48, no. 20, pp. 12435–12444, 2014, doi: 10.1021/es503790k.

[28] D. Bharadwaj, T. M. Fyles, and H. Struchtrup, "Multistage Pressure-Retarded Osmosis," *J. Non-Equilibrium Thermodyn.*, vol. 41, no. 4, pp. 327–347, 2016, doi: 10.1515/jnet-2016-0017.

[29] H. Manzoor, M. A. Selam, F. Bin Abdur Rahman, S. Adham, M. Castier, and A. Abdel-Wahab, "A tool for assessing the scalability of pressure-retarded osmosis (PRO) membranes," *Renew. Energy*, vol. 149, no. xxxx, pp. 987–999, 2020, doi: 10.1016/j.renene.2019.10.098.

[30] A. Zuber, R. F. Checoni, R. Mathew, J. P. L. Santos, F. W. Tavares, and M. Castier, "Thermodynamic Properties of 1:1 Salt Aqueous Solutions with the Electrolattice Equation of State A.," *Oil Gas Sci. Technol.*, vol. 68, no. 2, pp. 255–270, 2013, doi: 10.2516/ogst/2012088.

[31] M. Born, "Volumen und Hydratationswärme der Ionen," *Zeitschrift für Phys.*, vol. 1, no.

1, pp. 45–48, 1920, doi: 10.1007/BF01881023.

[32] L. Blum, “Mean spherical model for asymmetric electrolytes I. Method of solution,” *Mol. Phys.*, vol. 30, no. 5, pp. 1529–1535, 1975, doi: 10.1080/00268977500103051.

[33] H. Manzoor, *Simulation Of Full-Scale Pressure Retarded Osmosis Processes*. 2019.

[34] Saly Monir Matta, *Modeling The Performance Of Spiral-Wound Membranes In A Pressure-Retarded Osmosis Process*, No. May. Submitted to the Office of Graduate and Professional Studies of Texas A&M University in partial fulfillment of the requirements for the degree of Master Of Science, 2021.

[35] R. Turton, *Analysis, Synthesis, and Design of Chemical Processes Fourth Edition*, vol. 53, no. 9. 2013.

[36] S. Y. Ereev and M. K. Patel, “Standardized cost estimation for new technologies (SCENT) - methodology and tool,” *J. Bus. Chem.*, vol. 9, no. 1, pp. 31–48, 2012.

[37] S. Perry, R. H. Perry, D. W. Green, and J. O. Maloney, *Perry’s chemical engineers’ handbook*, vol. 38, no. 02. 2000.

[38] G. Towler and R. Sinnott, *Chemical Engineering Design. Principles, practice and economics of plant and process design*. 2008.

[39] M. S. Peters and J. I. Peters, *Plant design and economics for chemical engineers*, vol. 5, no. 1. 1959.

[40] N. Voutchkov and N. Voutchkov, “Cost Estimates – Types and Accuracy,” *Desalin. Proj. Cost Estim. Manag.*, no. 2018, pp. 57–64, 2019, doi: 10.1201/9781351242738-3.

[41] “The Chemical Engineering Plant Cost Index - Chemical Engineering.” https://www.chemengonline.com/pci-home (accessed Oct. 15, 2021).

[42] B. J. Feinberg, “Scale-up characteristics of salinity gradient power technologies,” UNIVERSITY OF CALIFORNIA Los Angeles, 2014.

[43] Y. yue Lu, Y. dong Hu, D. mei Xu, and L. ying Wu, “Optimum design of reverse osmosis seawater desalination system considering membrane cleaning and replacing,” *J. Memb. Sci.*, vol. 282, no. 1–2, pp. 7–13, 2006, doi: 10.1016/j.memsci.2006.04.019.

[44] J. Benjamin, M. E. Arias, and Q. Zhang, “A techno-economic process model for pressure retarded osmosis based energy recovery in desalination plants,” *Desalination*, vol. 476, no. November 2019, 2020, doi: 10.1016/j.desal.2019.114218.

[45] V. S. T. Sim, Q. She, T. H. Chong, C. Y. Tang, A. G. Fane, and W. B. Krantz, “Strategic co-location in a hybrid process involving desalination and pressure retarded osmosis (PRO),” *Membranes (Basel).*, vol. 3, no. 3, pp. 98–125, 2013, doi: 10.3390/membranes3030098.

[46] N. Voutchkov and N. Voutchkov, “Operation and Maintenance Costs,” *Desalin. Proj. Cost Estim. Manag.*, no. 2018, pp. 111–140, 2019, doi: 10.1201/9781351242738-5.

[47] K. Lutchmiah, A. R. D. Verliefde, K. Roest, L. C. Rietveld, and E. R. Cornelissen, “Forward osmosis for application in wastewater treatment: A review,” *Water Res.*, vol. 58, no. 0, pp. 179–197, 2014, doi: 10.1016/j.watres.2014.03.045.

[48] A. P. Straub, A. Deshmukh, and M. Elimelech, “Pressure-retarded osmosis for power generation from salinity gradients: Is it viable?,” *Energy Environ. Sci.*, vol. 9, no. 1, pp. 31–48, 2016, doi: 10.1039/c5ee02985f.

[49] M. G. Marcovecchio, P. A. Aguirre, and N. J. Scenna, “Global optimal design of reverse osmosis networks for seawater desalination: Modeling and algorithm,” *Desalination*, vol. 184, no. 1–3, pp. 259–271, 2005, doi: 10.1016/j.desal.2005.03.056.

[50] J. R. Ziolkowska, “Is Desalination Affordable?—Regional Cost and Price Analysis,” *Water Resour. Manag.*, vol. 29, no. 5, pp. 1385–1397, 2015, doi: 10.1007/s11269-014-0901-y.

[51] “Maintenance.” https://www.lenntech.com/maintenance.htm (accessed Apr. 11, 2021).

[52] Sandia National Laboratories, “Dakota Downloads | Dakota.” https://dakota.sandia.gov/download.html (accessed Jan. 16, 2021).

[53] H. Manzoor, M. A. Selam, S. Adham, H. K. Shon, M. Castier, and A. Abdel-Wahab, “Energy recovery modeling of pressure-retarded osmosis systems with membrane modules compatible with high salinity draw streams,” *Desalination*, vol. 493, no. April, p. 114624, 2020, doi: 10.1016/j.desal.2020.114624.

[54] M. Li, “Analysis and Optimization of Pressure Retarded Osmosis for Power Generation,” *AIChE J.*, vol. 59, no. 4, pp. 215–228, 2012, doi: 10.1002/aic.

[55] A. P. Straub, N. Y. Yip, and M. Elimelech, “Raising the Bar: Increased Hydraulic Pressure Allows Unprecedented High Power Densities in Pressure-Retarded Osmosis,” *Environ. Sci. Technol. Lett.*, vol. 1, no. 1, pp. 55–59, 2013, doi: 10.1021/ez400117d.

[56] I. R. E. Agency, *Renewable Power Generation Costs in 2019*. 2020.

[57] S. Ho Chae, Y. M. Kim, H. Park, J. Seo, S. J. Lim, and J. H. Kim, “Modeling and simulation studies analyzing the pressure-retarded osmosis (PRO) and pro-hybridized processes,” *Energies*, vol. 12, no. 2, pp. 1–35, 2019, doi: 10.3390/en12020243.

[58] H. T. Madsen, S. S. Nissen, J. Muff, and E. G. Søgaard, “Pressure retarded osmosis from hypersaline solutions: Investigating commercial FO membranes at high pressures,” *Desalination*, vol. 420, no. March, pp. 183–190, 2017, doi: 10.1016/j.desal.2017.06.028.

[59] J. H. L. V Quantum J. Wei, Ronan K. McGovern, “Saving energy with an optimized

two-stage reverse osmosis system," *R. Soc. Chem.*, 2018.

[60] A. Zhu, A. Rahardianto, P. D. Christofides, and Y. Cohen, "Reverse osmosis desalination with high permeability membranes - Cost optimization and research needs," *Desalin. Water Treat.*, vol. 15, no. 1–3, pp. 256–266, 2010, doi: 10.5004/dwt.2010.1763.

[61] A. Zhu, P. D. Christofides, and Y. Cohen, "Effect of thermodynamic restriction on energy cost Optimization of RO membrane water desalination," *Ind. Eng. Chem. Res.*, vol. 48, no. 13, pp. 6010–6021, 2009, doi: 10.1021/ie800735q.

[62] H. W. Chung, J. Swaminathan, and J. H. Lienhard, "Multistage pressure-retarded osmosis configurations: A unifying framework and thermodynamic analysis," *Desalination*, vol. 476, no. November 2019, p. 114230, 2020, doi: 10.1016/j.desal.2019.114230.

[63] D. Tondeur and E. Kvaalen, "Equipartition of Entropy Production. An Optimality Criterion for Transfer and Separation Processes," *Ind. Eng. Chem. Res.*, vol. 26, no. 1, pp. 50–56, 1987, doi: 10.1021/ie00061a010.

[64] J. H. V. Lienhard, "Energy Savings in Desalination Technologies: Reducing Entropy Generation by Transport Processes," *J. Heat Transfer*, vol. 141, no. 7, pp. 1–11, 2019, doi: 10.1115/1.4043571.

[65] A. Altaee and N. Hilal, "Dual stage PRO power generation from brackish water brine and wastewater effluent feeds," *Desalination*, vol. 389, pp. 68–77, 2016, doi: 10.1016/j.desal.2015.03.033.

[66] M. Li, "Systematic analysis and optimization of power generation in pressure retarded osmosis: Effect of multistage design," *AIChE J.*, vol. 64, no. 1, pp. 144–152, 2018, doi: 10.1002/aic.15894.

[67] W. He, Y. Wang, and M. H. Shaheed, “Enhanced energy generation and membrane performance by two-stage pressure retarded osmosis (PRO),” *Desalination*, vol. 359, pp. 186–199, 2015, doi: 10.1016/j.desal.2014.12.014.

APPENDIX 1: FLOWCHART FOR SOLVING CO-CURRENT FLOW ACCOUNTING FOR VARIATIONS ALONG THE MEMBRANE

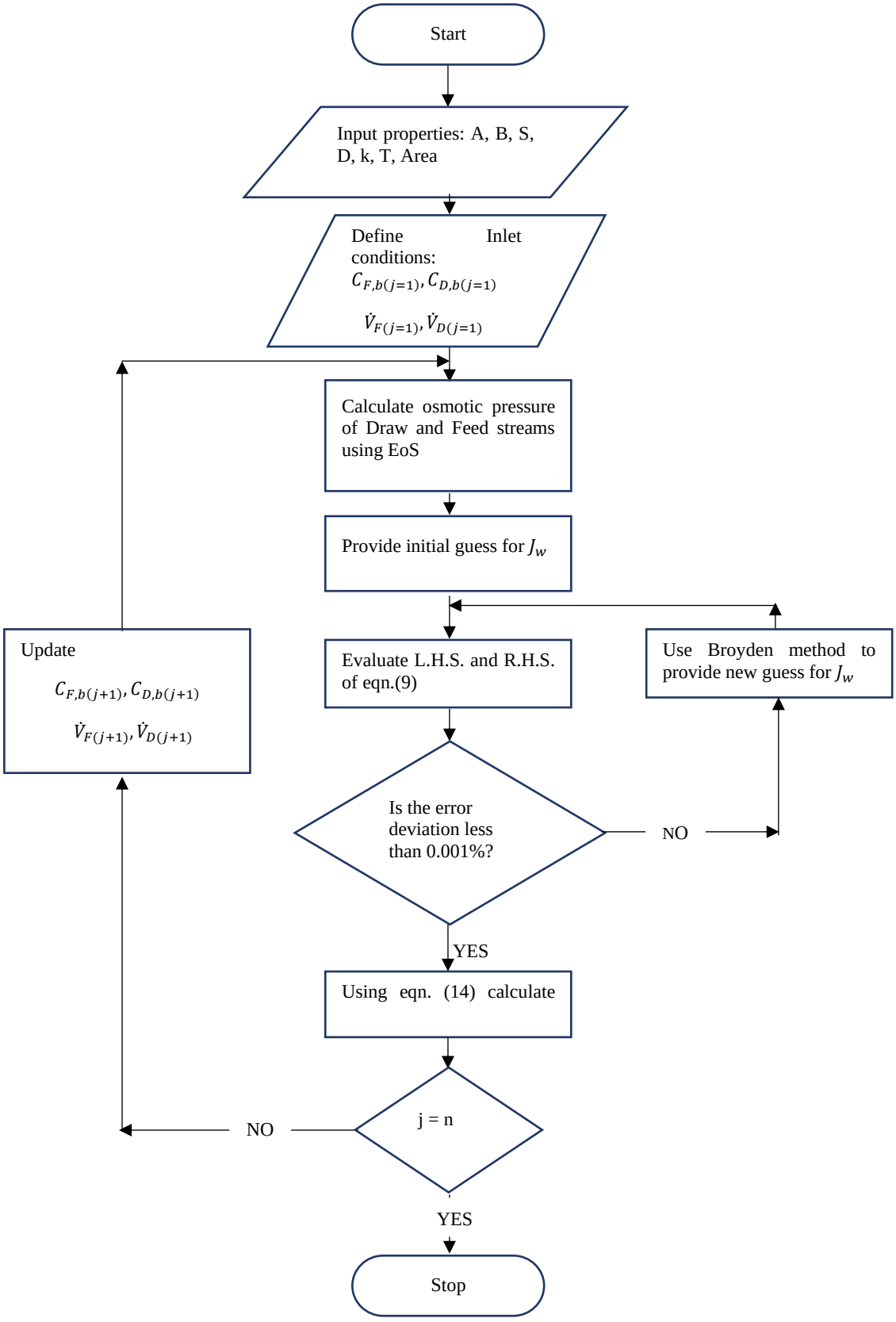

APPENDIX 2: FLOWCHART FOR SOLVING COUNTER-CURRENT FLOW CONFIGURATION

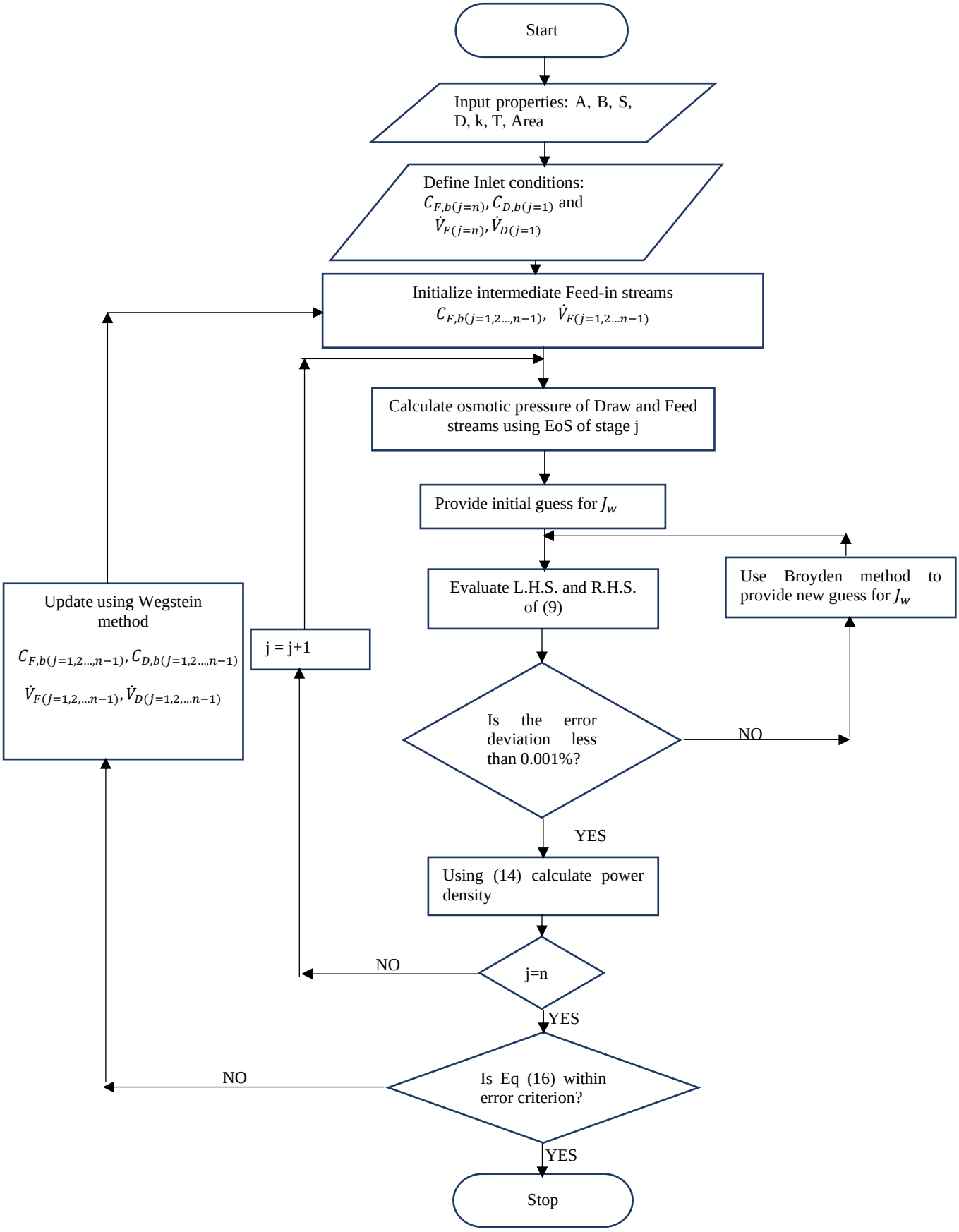

APPENDIX 3: CALCULATION PROCEDURE FOR SPIRAL WOUND MEMBRANE